Fraunhofer Institut
Techno- und
Wirtschaftsmathematik

S. Rief

Modeling and simulation of the pressing section of a paper machine

Berichte des Fraunhofer ITWM, Nr. 113 (2007)

ISSN 1434-9973

Bericht 113 (2007)

Die Veröffentlichungen in der Berichtsreihe des Fraunhofer ITWM können bezogen werden über:

Fraunhofer-Institut für Techno- und
Wirtschaftsmathematik ITWM
Fraunhofer-Platz 1

67663 Kaiserslautern
Germany

Telefon: +49 (0) 6 31/3 16 00-0
Telefax: +49 (0) 6 31/3 16 00-10 99
E-Mail: info@itwm.fraunhofer.de
Internet: www.itwm.fraunhofer.de

Vorwort

Das Tätigkeitsfeld des Fraunhofer-Instituts für Techno- und Wirtschaftsmathematik ITWM umfasst anwendungsnahe Grundlagenforschung, angewandte Forschung sowie Beratung und kundenspezifische Lösungen auf allen Gebieten, die für Techno- und Wirtschaftsmathematik bedeutsam sind.

In der Reihe »Berichte des Fraunhofer ITWM« soll die Arbeit des Instituts kontinuierlich einer interessierten Öffentlichkeit in Industrie, Wirtschaft und Wissenschaft vorgestellt werden. Durch die enge Verzahnung mit dem Fachbereich Mathematik der Universität Kaiserslautern sowie durch zahlreiche Kooperationen mit internationalen Institutionen und Hochschulen in den Bereichen Ausbildung und Forschung ist ein großes Potenzial für Forschungsberichte vorhanden. In die Berichtreihe sollen sowohl hervorragende Diplom- und Projektarbeiten und Dissertationen als auch Forschungsberichte der Institutsmitarbeiter und Institutsgäste zu aktuellen Fragen der Techno- und Wirtschaftsmathematik aufgenommen werden.

Darüber hinaus bietet die Reihe ein Forum für die Berichterstattung über die zahlreichen Kooperationsprojekte des Instituts mit Partnern aus Industrie und Wirtschaft.

Berichterstattung heißt hier Dokumentation des Transfers aktueller Ergebnisse aus mathematischer Forschungs- und Entwicklungsarbeit in industrielle Anwendungen und Softwareprodukte – und umgekehrt, denn Probleme der Praxis generieren neue interessante mathematische Fragestellungen.

Prof. Dr. Dieter Prätzel-Wolters
Institutsleiter

Kaiserslautern, im Juni 2001

Modeling and Simulation of the Pressing Section of a Paper Machine

Stefan Rief, Fraunhofer ITWM, Kaiserslautern, Germany
stefan.rief@itwm.fraunhofer.de

May 21, 2007

Abstract

We are concerned with modeling and simulation of the pressing section of a paper machine. We state a two-dimensional model of a press nip which takes into account elasticity and flow phenomena. Nonlinear filtration laws are incorporated into the flow model. We present a numerical solution algorithm and a numerical investigation of the model with special focus on inertia effects.

Keywords. paper machine, computational fluid dynamics, porous media

1 Introduction

The paper machine is a huge piece of equipment reaching width and height of 12 meters and length of up to 250 meters, respectively. Typically, it consists of four main parts: the headbox, the sheet forming section, the pressing section and the drying section (see Figure 1).

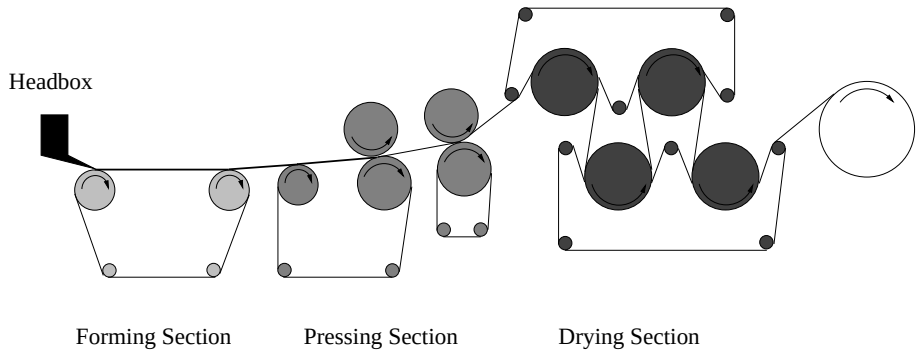

Figure 1: Paper machine

The headbox provides the fiber suspension having approximately 99 percent fluid content. From the headbox the suspension enters the sheet forming section at high speeds of up to 2000 m/min. On a woven structure called forming fabric dewatering starts by natural filtration. Additional suction boxes may support the dewatering process, such that the fluid content is decreased to about 80 percent at the entrance of the pressing section. By means of dewatering felts the paper layer is transported through several press nips. A press nip in its simplest form consists of two rolls which compress the paper-felt sandwich (see Figure 2).
Since the felt is a porous structure providing void space, the fluid is squeezed out from the paper and enters the felt. Thereby, the fluid content is decreased to approximately 50 percent when the paper reaches the drying section. Here, further dewatering is accomplished by evaporation. Steam-heated cylinders over which the paper layer is transported reduce the fluid content to 5 percent. In the end, the paper is stored on huge rolls ready for further processing like coating or cutting.

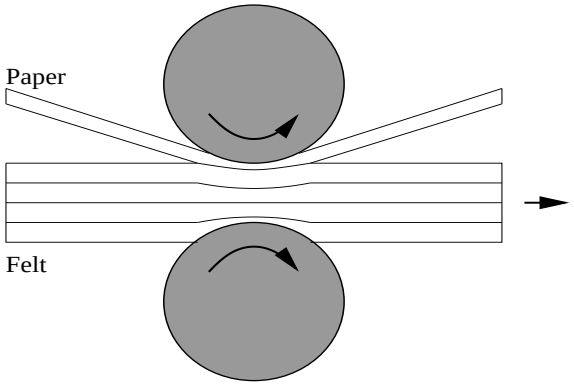

Figure 2: Roll press nip

In the abstract of [8], a summary of the current state of research in the paper making industry is given. It is stated, that in the paper making industry process optimization has almost always taken place by tests and measurements. Nevertheless, this trial and error approach has led to the situation that no drastic improvements can be expected in the future. But, due to the huge amount of paper being typically produced in a paper mill, even small improvements can save a lot of money and energy. To achieve progress nowadays, more detailed understanding of the dewatering processes is needed. Besides further development of experimental methods and running expensive measurement series on test paper machines, mathematical modeling and computer simulation can be the tools to support R & D in the paper making industry. One intrinsic property of modeling and simulation is that these methods are not limited to existing paper machines and

clothings, but they can also be used as tools to predict the behavior of completely new designs. On the other hand, modeling and simulation will not replace measurements. They are still needed as a link to reality to provide ways for validation of the models and to give hints to empirical laws where modeling from first principles is too complicated.
We completely agree with this assessment except for the statement that no drastic improvements could be achieved. Looking at dewatering felts, we observe that the manufacturing process does not operate at the length scale of micrometers, but merely at millimeters. Typically, a felt consists of a woven structure called base weave. It is made of yarns which may reach diameters of 0.2 mm to 2.0 mm. A needling process attaches several layers of fine fibers to the base weave. The diameters of the fine fibers are between 10 μm and 80 μm. The needling process creates a very irregular structure which is by no means fluid dynamically or elastically optimized. Being able to manufacture at the micro scale yields great potential for future improvements and, as already mentioned above, computer simulation can play a keyrole in predicting the optimum material properties.
In this report, we focus on the simulation of press nips in the pressing section. Since mechanical drying is considered to be ten times cheaper than thermal drying, a lot of energy and money can be saved by improved dewatering felts and optimum press profiles. Moreover, better drying rates insure higher quality of the final product, since its elastic strength is increased. Another advantage is the fact that the paper machine may operate at higher speeds still delivering the needed heating capacity in the drying section. Hence, there is an increase in productivity of the paper machine.
In the next section, we consider the pressing section of a paper machine and establish a mathematical model describing the elastic and fluid dynamical behavior of the paper-felt sandwich when passing a press nib. In contrast to [8] and [14], the model is two-dimensional as it neglects only the cross direction of the paper machine. The paper and felt layers are considered to be porous media. Due to high pressure gradients in the nip the fluid velocities reach high levels where Darcy's law is not applicable anymore. Therefore, the model allows for the use of nonlinear filtration laws extending existing models like in [7]. In Section 3, we describe the solution algorithms of the model equations and the discretization. Section 4 is devoted to model parameters, since they turn out to be a crucial part of the simulations. For example, we use the methods developed in [11] and compute nonlinear macroscopic filtration laws. Therefore, we extend the methods to a three-dimensional felt structure which is generated by GeoDict, a virtual structure generator developed at Fraunhofer ITWM, Kaiserslautern. The three-dimensional flow field is then computed by ParPac which is a parallel lattice Boltzmann solver also developed at Fraunhofer ITWM. We close this report by a presentation of numerical results.

2 Model of a press nip

As mentioned in the previous section, the pressing section of a paper machine consists of several press nips. Nowadays, there exist two different types of press nips. In Figure 2 a sketch of a roll press nip is drawn. Figure 3 shows a modern shoe press nip. Its advantage is the enhanced press zone due to a concave-convex combination of the opposing press profiles.

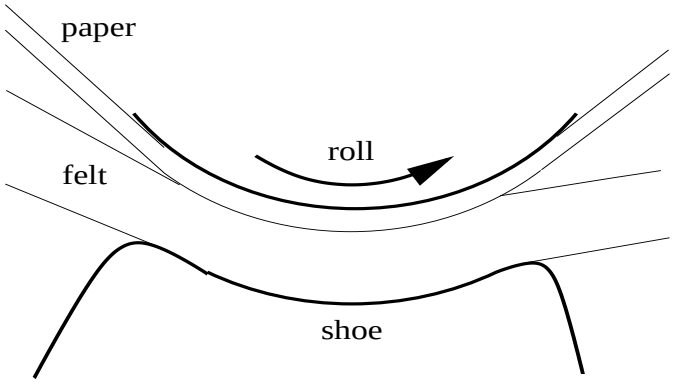

Figure 3: Shoe press

Typically, the press zone of a roll press nip reaches lengths between 40 mm and 70 mm, whereas a shoe press may reach up to 300 mm. In contrast, the felt thickness is usually less then 4 mm and the paper thickness may go down to 100 micrometers. The paper-felt sandwich is squeezed between the press profiles. Thereby, the fluid from the fibrous paper layer enters the porous felt structure, hence dewatering takes place. Two essential phenomena characterizing the dewatering process are elasticity and fluid dynamics. Our model of a press nip is quiet similar to the model developed in [14]. Nevertheless, it is extended to two dimensions and nonlinear filtration laws are incorporated. The derivation of the model is not entirely based on first principles and mathematically rigorous considerations. In addition to the derivations in [11], i.e. the flow equations in a periodic porous medium in case of high velocities and full saturation, phenomenological and empirical laws are used. The reason is twofold. To the best of the author's knowledge, there does not exist a rigorous mathematical derivation of effective two-phase flow equations in porous media. In case of elasticity, a computer model on the fiber level is very complicated since contact problems including friction have to be considered. Even if a computer model were available, determining its input parameters is not easy.
As indicated in Figure 2 and Figure 3, let's assume that the felt passes the press nip from the left to the right. This direction is called *machine direction* (MD) and will be referred to as x direction in this chapter. The y

direction is aligned to the axes of the rolls and is called *cross direction* (CD). The z direction is called transversal direction (TD). Since the length of the cylindric roll is up to 12 m and, therefore, much larger than the press zone in MD and the paper-felt sandwich in ZD, the cross direction is neglected.

2.1 Elasticity model

To describe the elastic behavior of the felt, we follow a phenomenological approach. Due to the highly demanding process conditions, the felt is by construction very stiff in machine direction. Therefore, we consider deformation only in transversal direction. Guided by measurements, we assume that the felt behaves viscoelastically which is, indeed, a widely accepted assumption (see [14] and references therein). Motivated by [9], the paper layer is modeled quite similar to the felt layers. In contrast to the felt, the paper layer does not recover completely after the press nip. This is due to plastic deformation. It keeps a permanent compression which adds a new parameter to the model. The ordinary differential equations which describe the deformation in transversal direction when passing through the nip read:

$$\begin{aligned} \tau(t) &= E_1(\varepsilon_1(t)) + \Lambda_1 \frac{d}{dt} E_1(\varepsilon_1(t)) - K \cdot \tau_{max}(t), \qquad (1) \\ \tau(t) &= E_i(\varepsilon_i(t)) + \Lambda_i \frac{d}{dt} E_i(\varepsilon_i(t)), \qquad i = 2, \ldots, n. \end{aligned}$$

The preceding equations are a system of Kelvin-Voigt laws for n layers. The strain is denoted by $\varepsilon_i(t) = \frac{l_i(t) - l_{0,i}}{l_{0,i}}$, where $l_{0,i}$ is the undeformed thickness of layer i and $l_i(t)$ is the deformed thickness at time t. The stress measured in $[Pa]$ is denoted by τ. Note, that τ is independent of the layers and just a function of t. Moreover, the functions E_i relating the elastic part of the stress and the strains ε_i might be nonlinear. Λ_i (in [s]) are viscoelastic time constants which determine the speed of relaxation. In (1), the first equation describes the paper layer. Therefore, we observe the additional term, which introduces a permanent deformation. This term depends linearly by the constant K on the maximum stress to which the paper has been exposed. The maximum stress is given by

$$\tau_{max}(t_0) := \max_{t \le t_0} \tau(t).$$

By using the relation $x = c * t$, where $c = \|\mathbf{v}_s\|$, and assuming negligible rigid body motion of the layers in transversal direction, we can eliminate the time variable and get

$$\begin{aligned} \tau(x) &= E_1(\varepsilon_1(x)) + \Lambda_1 c \frac{d}{dx} E_1(\varepsilon_1(x)) - K \cdot \tau_{max}(x), \qquad (2) \\ \tau(x) &= E_i(\varepsilon_i(x)) + \Lambda_i c \frac{d}{dx} E_i(\varepsilon_i(x)), \qquad i = 2, \ldots, n. \end{aligned}$$

Clearly, we have

$$\tau_{max}(x_0) := \max_{x \le x_0} \tau(x). \tag{3}$$

As indicated by Figure 4, the two press profiles are positioned by using d_{min} which is the minimum distance between the profiles. d_{min} is an input parameter of the problem. Due to the viscoelastic behavior of the porous layers, the overall thickness of the paper-felt sandwich will never exceed its initial undeformed thickness l_0. Therefore, the function

$$f(x) := \min(l_0, \text{distance of press profiles at position } x) \tag{4}$$

is well-defined and, in addition to (2), (3), the following relation holds true

$$\sum_{i=1}^{n} \varepsilon_i(x) l_{0,i} = l_0 - f(x). \tag{5}$$

The deformation process can be subdivided into three phases (see Figure 4):

- *Phase 0* ($x_i \le x \le x_r$): no deformation; vertical position is specified by input parameter z_i;
- *Phase 1* ($x_r \le x \le x_l$): viscoelastic deformation ruled by (2),..., (5), x_l is computed by the condition $\tau(x_l) = 0$;
- *Phase 2* ($x_l \le x \le x_o$): as *Phase 1*, but τ is equal to zero; vertical position given by z_o (z coordinate of lower press profile at x_l).

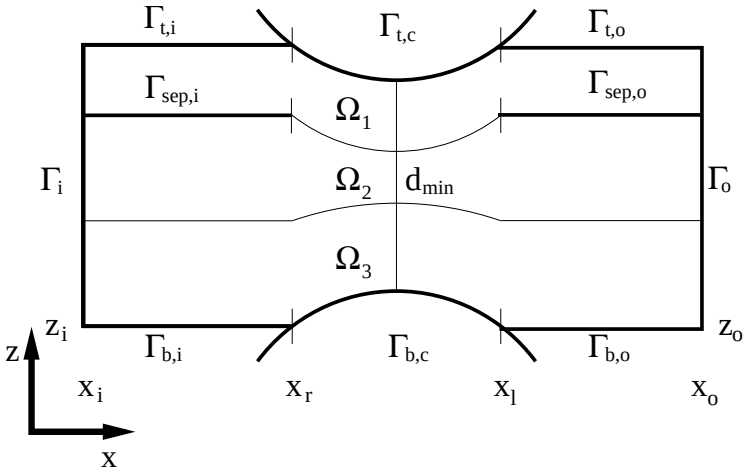

Figure 4: Terminology

We want to point out that there is no coupling of elasticity and fluid dynamics. For instance, we neglect the influence of the fluid pressure on the felt deformation. Furthermore, we assume that the deformation results in a temporary rearrangement of fibers rather than in a compression of fibers. Therefore, the solid phase is assumed to be incompressible. Incompressibility allows for a simple computation of the porosity, once the strain is known. Let $\Phi_{0,i}$ and Φ_i be the initial and deformed porosity of layer i, respectively. Incompressibility of the solid phase means

$$(1 - \Phi_{0,i})l_{0,i} \quad = \quad (1 - \Phi_i(x))l_i(x).$$

Using the definition of strain yields

$$(1 - \Phi_{0,i}) \quad = \quad (1 - \Phi_i(x))(1 + \varepsilon_i(x)),$$

and, finally,

$$\Phi_i(x) = \frac{\varepsilon_i(x) + \Phi_{0,i}}{1 + \varepsilon_i(x)}. \tag{6}$$

2.2 Flow model

The fibrous paper layer and the different layers of the felt, i.e. base weave and batt fiber layers consisting of fine fibers, are modeled as porous media. In the following, we will refer to the fluid and solid constituents of a porous medium as *fluid phase* and *solid phase* indexed by 'f' and 's', respectively. Since the pore space of a felt is not entirely filled by fluid, there is an additional gaseous phase indexed by 'g'. The three phases are treated as a mixture of overlapping continua (see [1]). This approach considers the variables of each phase to be defined everywhere in the physical domain which is from a macroscopic point of view a reasonable assumption.
In the framework of overlapping continua, the momentum balance equation for the fluid phase reads

$$\Phi_f \rho_f \frac{\mathrm{D}_f \mathbf{v}_f}{\mathrm{D}\, t} - \nabla \cdot \mathbf{t}_f - \Phi_f \rho_f \mathbf{b}_f = \mathbf{m}_f, \tag{7}$$

where

$$\frac{\mathrm{D}_f}{\mathrm{D}\, t} = \frac{\partial}{\partial t} + \mathbf{v}_f \cdot \nabla$$

denotes the material derivative. In (7), the volume fraction of the fluid phase is denoted by Φ_f. ρ_f is the intrinsic fluid density in $[\frac{kg}{m^3}]$. The fluid velocity measured in $[\frac{m}{s}]$ is abbreviated by $\mathbf{v}_f$. $\mathbf{t}_f$ is the stress tensor in $[Pa]$. The unit of the specific body force $\mathbf{b}_f$ is $[\frac{N}{kg}]$ and the term describing the rate of momentum exchange into the fluid phase is denoted by $\mathbf{m}_f$ and is measured in $[\frac{N}{m^3}]$.

We assume negligible gravity, a Newtonian fluid, slow flow (for the moment) and Stokes drag as model of interaction of solid and fluid phase. Then, the stationary form of equation (7) reads

$$\Phi_f(\mathbf{v}_f - \mathbf{v}_s) = -\frac{\mathbf{K}_f}{\mu_f} \cdot \nabla p_f. \tag{8}$$

μ_f is the dynamic viscosity in $[Pa\,s]$. $\mathbf{K}_f$ denotes the permeability tensor in $[m^2]$. The hydrodynamic pressure p_f is measured in $[Pa]$. $\mathbf{v}_s$ is the velocity of the solid phase.
Equation (8) is a two-phase version of Darcy's law in the case of a moving porous medium. It is supplemented by the stationary mass balance equation

$$\nabla(\Phi_f \mathbf{v}_f) = 0. \tag{9}$$

Although not made explicit, all model parameters may depend on the space variables x and z, since the layer properties which they describe may differ. For the gaseous phase, we apply Richards' assumption, which states that the air has a negligible influence on the fluid and solid phases. Mathematically, this assumption is expressed by setting p_g equal to zero, i.e. p_g is set to atmospheric pressure. Richards' assumption is justified by the fact, that air has a much smaller viscosity than the fluid and is very *mobile*. In fact, to achieve even larger air mobilities in paper manufacturing, surface chemicals are added. Clearly, some phenomena like fluid enclosed air bubbles are neglected by this approach.
To close our flow model (8), (9), we introduce the notion of capillary pressure, porosity and saturation. The capillary pressure is defined by

$$p_c := p_g - p_f.$$

Since, $p_g = 0$, we simply have

$$p_c = -p_f.$$

The ratio between void and total volume of a porous medium is called porosity Φ. The saturation S indicates how much of the void volume is occupied by the fluid phase. It is defined by

$$S = \frac{\Phi_f}{\Phi}.$$

Experimental observations show, that there exists a relation between capillary pressure and saturation. In porous media theory (see [3], [5]), it is therefore quite common to use this relation as additional constitutive model equation. Influenced by steady state measurements using real dewatering felts, we choose the following relation:

$$S(p_f) = \begin{cases} \left(\frac{1}{1-s_\infty} + \left(\frac{p_f}{a}\right)^2\right)^{-1} + s_\infty, & \text{if } p_f \le 0, \\ 1, & \text{if } p_f > 0, \end{cases} \tag{10}$$

where p_c is already substituted by $-p_f$. s_∞ is the residual saturation as p_f tends to $-\infty$. $a \in \mathbb{R}^-$ is an additional shape parameter which will be used to adjust different saturations in the felt layers at a given pressure level (see Figure 5).

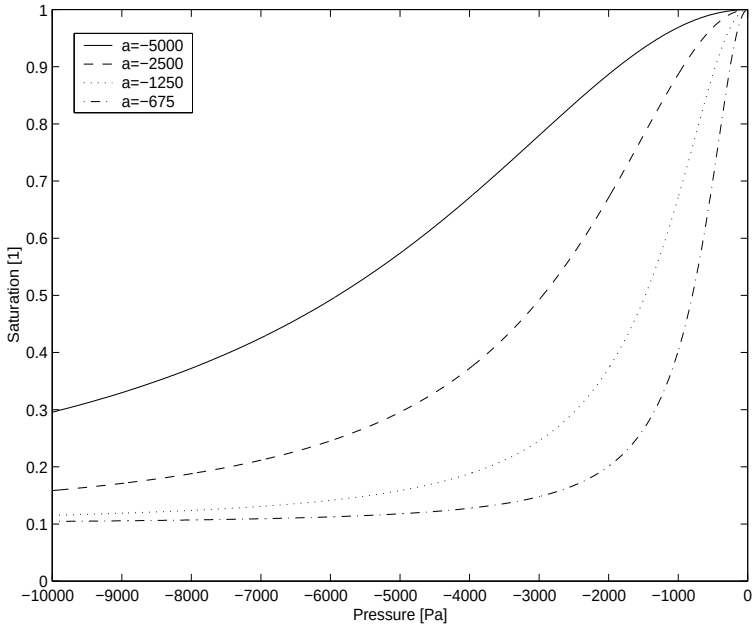

Figure 5: Retention curve: Variation of the parameter a ($s_\infty = 0.1$)

In (8), $\mathbf{K}_f$ can not be assumed constant, since porosity and saturation will vary significantly during compression and relaxation. Therefore, we assume

$$\mathbf{K}_f(\Phi, S) = \mathbf{K}_f^0 \frac{\Phi^3}{1-\Phi^2} S^b. \tag{11}$$

The factor $\Phi^3/(1-\Phi^2)$ originates from the Kozeny-Karman relation (see [4]). $1 \leq b \in \mathbb{R}$ is a shape parameter. In (11) the term S^b decreases permeability as the saturation is less than 1. This is a reasonable assumption, since $\mathbf{K}_f$ is then a relative permeability. The permeability tensor $\mathbf{K}_f^0$ can be interpreted as the medium's permeability when the porosity is approximately 0.775 and when the medium is fully saturated.
Let us assume that the porosity is given by the deformation model. The flow model (8), ...,(11) is then closed. Indeed, applying the divergence operator to (8), using the mass balance equation (9) and by simple substitutions, we obtain one nonlinear partial differential equation for the fluid pressure p_f:

$$-\operatorname{div}\Big(S(p_f)\Phi\mathbf{v}_s\Big) = -\operatorname{div}\Big(\frac{\mathbf{K}_f^0}{\mu_f}\frac{\Phi^3}{1-\Phi^2}S(p_f)^b \cdot \nabla p_f\Big). \tag{12}$$

After computing p_f, (8) can be employed to calculate the fluid velocities. Now, we want to include nonlinear filtration laws in our model. The filtration laws which are derived in [11] are only valid in the case of full saturation. Hence, we define

$$\mathcal{F}_0^{\mathrm{nl}}(\nabla p_f, \Phi) := \begin{cases} \mathcal{F}^{\mathrm{nl}}(\nabla p_f, \Phi), & \text{if } S = 1, \\ 0, & \text{if } S < 1. \end{cases} \tag{13}$$

The modified equation (8) reads

$$\Phi_f(\mathbf{v}_f - \mathbf{v}_s) = -\frac{\mathbf{K}_f}{\mu_f} \cdot \nabla p_f + \mathcal{F}_0^{\mathrm{nl}}(\nabla p_f, \Phi). \tag{14}$$

Using (14) instead of (8) in the above consideration, we obtain the following partial differential equation for p_f:

$$\begin{aligned} &- \operatorname{div}\Big(S(p_f)\Phi \mathbf{v}_s \Big) \\ &= - \operatorname{div}\Big(\tfrac{\mathbf{K}_f^0}{\mu_f} \tfrac{\Phi^3}{1-\Phi^2}\, S(p_f)^b \cdot \nabla p_f - \mathcal{F}_0^{\mathrm{nl}}(\nabla p_f, \Phi) \Big). \end{aligned} \tag{15}$$

It is a nonlinear elliptic partial differential equation if $\mathbf{v}_s$ is sufficiently small. It has to be supplemented by suitable Dirichlet and Neumann boundary conditions. The different parts of the boundary are shown in Figure 4 in the case of a roll press nip. Nevertheless, the terminology also applies to shoe presses. It is assumed, that Ω_1 is the paper layer. Provided that Γ_i is sufficiently far away from the center of the nip, it is reasonable to prescribe the saturation $S_{0,i}$ of each porous layer there. Using (10), one gets Dirichlet conditions for the pressure which are uniquely defined if the prescribed saturations are less than 1. This is always the case in real life. Moreover, we assume the system of layers to be in equilibrium, i.e. there is no fluid exchange between layers. Therefore, the Dirichlet conditions are even constant. Again, if Γ_o is sufficiently far away from the center of the nip, it is natural to assume the normal component of the relative velocity $\mathbf{v}_f - \mathbf{v}_s$ to be zero. By the aid of (14) one obtains a homogeneous Neumann boundary condition for p_f. Vanishing normal components of the fluid velocity are applied to all of the remaining parts of the boundary. Since the normal component of the solid velocity is zero on these parts, we have again a homogeneous Neumann boundary condition. On the parts of the boundary where the paper-felt sandwich is in contact to the press profiles, i.e. $\Gamma_{i,c}$, $\Gamma_{b,c}$, this condition is correct since roll and shoe profiles are impervious. On $\Gamma_{t,i}$, $\Gamma_{b,i}$, $\Gamma_{t,o}$ and $\Gamma_{b,o}$ the situation may be different depending on process conditions. Observations show that fluid may escape through the top and bottom surface of the felt. In the simulations presented below, there is a very low pressure near these boundaries and, therefore, it is save to apply

homogeneous Neumann conditions. As shown in Figure 3, the paper and the felt are separated before and after the nip. We account for this fact by the introduction of $\Gamma_{sep,i}$ and $\Gamma_{sep,o}$.

2.3 Remark on roll surfaces and belts

Besides paper and felt layers, there appear other types of layers in the press nip. We additionally find grooved roll surfaces, roll surfaces with wholes and grooved shoe press belts. These layers provide void space for the fluid, thereby decreasing the hydrodynamic pressure. The length scale of the void space structure is much coarser than the micro structure of the felt and paper fibers. Nevertheless, we model them as porous media. Their porosity is given by the ratio of void and solid space. Their permeability is set orders of magnitude higher than the respective permeabilities of felt and paper layers. The reason behind is the fact, that very small flow resistivity is to be expected due to the coarse structure. Additionally, similar to the paper layer, we introduce separating boundaries, which are determined automatically by the computed values for x_r and x_l.

3 Numerical solution algorithms

In this section, we present the algorithmic structure and numerical methods to solve the model equations which are derived above. The flow chart in Figure 6 shows the sequence of basic solution steps.

3.1 Elasticity solver

First, the press geometry is created. For that purpose, the profiles are fixed in machine direction by suitable input parameters. The lower press profile is additionally fixed in transversal direction. Then, by using d_{min}, the position of the upper press can be computed.
Now, we enter *Phase 0* of the deformation simulation. z_i fixes the vertical position of the layers (see Figure 4). Starting at x_i, the x position is incremented, thereby monitoring the function f defined in (4). The first x position where f is smaller than l_0 determines x_r and *Phase 0* is finished. During the computation of x_r, there may be a *collision* of the porous layers and the press profiles. In that case, the horizontal fixation is done by aligning the layers to the collision press profile.
In *Phase 1*, the deformation is computed according to the model equations (2), ..., (5). To simplify the exposition, a linear elasticity law is chosen, i.e. $E_i(\varepsilon_i) = A_i \cdot \varepsilon_i$. The method can be extended with minor changes to laws of type $E_i(\varepsilon_i) = A_i \cdot \varepsilon_i^r$, $r \geq 1$. Equation (5) allows to express ε_1 in terms of

ε_i, $i = 2, \ldots, n$:

$$\varepsilon_1(x) = \frac{1}{l_{0,1}}(l_0 - f(x) - \sum_{i=2}^{n} \varepsilon_i(x) l_{0,i}). \tag{16}$$

Plugging (16) in the first equation of (2), yields a system in ε_i, $i = 2, \ldots, n$ and τ. τ is eliminated by subtracting the second equation in (2) from all others. Hence we have the following system of ordinary differential equations in ε_i, $i = 2, \ldots, n$:

$$\mathbf{A} \cdot \varepsilon' = \mathbf{B} \cdot \varepsilon + \mathbf{c}(x), \tag{17}$$

where $\mathbf{A}$ and $\mathbf{B}$ are $n-1$-quadratic matrices with constant entries and $\mathbf{c}(x)$ is a $n-1$-vector depending on x. $\varepsilon = (\varepsilon_2, \ldots, \varepsilon_n)^T$. More precisely, we have:

$$\mathbf{A} = \begin{pmatrix} \Lambda_2 c A_2 + \Lambda_1 c A_1 \frac{l_{0,2}}{l_{0,1}} & \Lambda_1 c A_1 \frac{l_{0,3}}{l_{0,1}} & \Lambda_1 c A_1 \frac{l_{0,4}}{l_{0,1}} & \ldots & \Lambda_1 c A_1 \frac{l_{0,n}}{l_{0,1}} \\ -\Lambda_2 c A_2 & \Lambda_3 c A_3 & 0 & \ldots & 0 \\ -\Lambda_2 c A_2 & 0 & \Lambda_4 c A_4 & \ldots & 0 \\ \vdots & & \ldots & & \vdots \\ -\Lambda_2 c A_2 & 0 & 0 & \ldots & \Lambda_n c A_n \end{pmatrix},$$

$$\mathbf{B} = \begin{pmatrix} -A_2 - A_1 \frac{l_{0,2}}{l_{0,1}} & -A_1 \frac{l_{0,3}}{l_{0,1}} & -A_1 \frac{l_{0,4}}{l_{0,1}} & \ldots & -A_1 \frac{l_{0,n}}{l_{0,1}} \\ A_2 & -A_3 & 0 & \ldots & 0 \\ A_2 & 0 & -A_4 & \ldots & 0 \\ \vdots & & \ldots & & \vdots \\ A_2 & 0 & 0 & \ldots & -A_n \end{pmatrix}$$

and

$$\mathbf{c}(x) = \begin{pmatrix} \frac{A_1}{l_{0,1}}(l_0 - f(x)) - \frac{\Lambda_1 c A_1}{l_{0,1}} f'(x) - K\tau_{max}(x) \\ 0 \\ \vdots \\ 0 \end{pmatrix}.$$

The matrix $\mathbf{A}$ is invertible, due to the fact that all parameters A_i, Λ_i, $l_{0,i}$ and c are strictly positive. Therefore, we can write (17) in canonical form

$$\varepsilon' = \mathbf{A}^{-1}\mathbf{B} \cdot \varepsilon + \mathbf{A}^{-1}\mathbf{c}(x). \tag{18}$$

This system is solved by the classical fourth-order Runge-Kutta method.

ELASTICITY SOLVER FLOW SOLVER

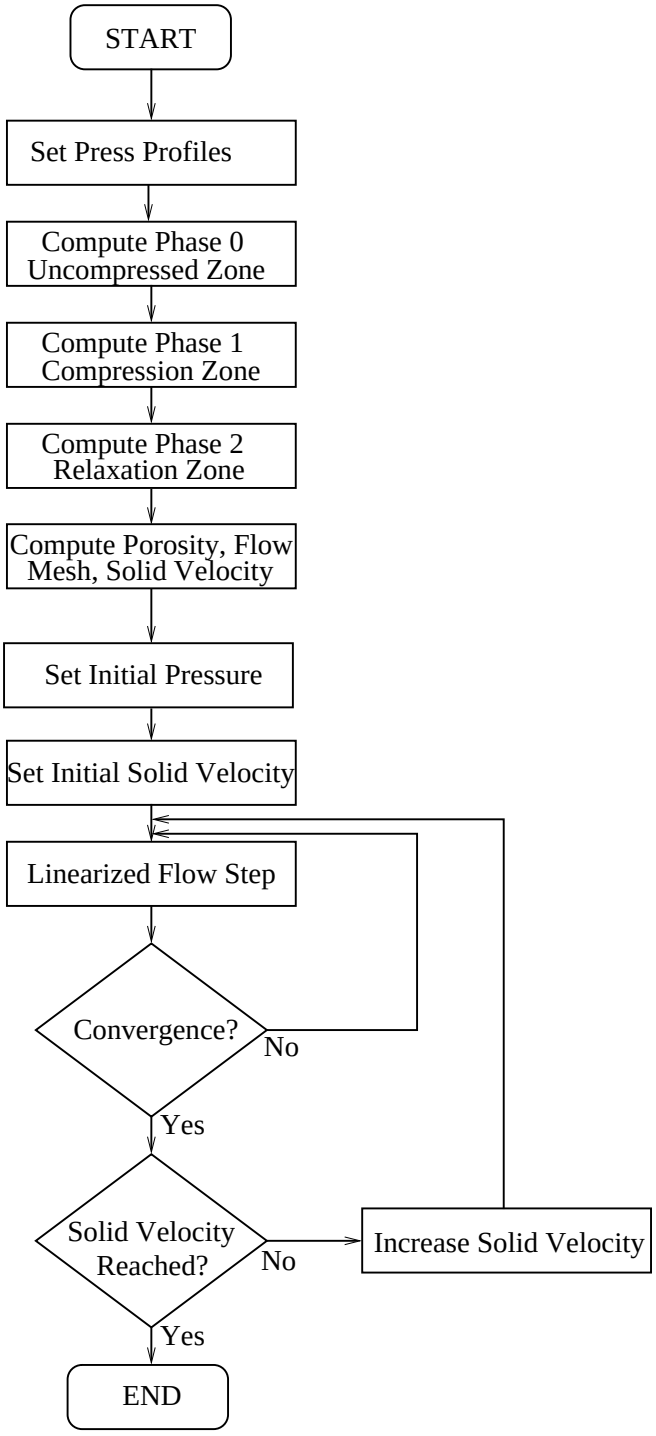

Figure 6: Flow chart of simulation steps

Initial conditions are given by

$$\varepsilon(x_l) = 0.$$

ε_1 and τ are computed using (16) and (2). By identifying the first zero of the function τ, we get the point x_r.

Remark 1 To solve the equations of *Phase 1*, f has to be differentiable. This is no further restriction of our model. Smoothness is a technical requirement to reduce wear and guarantee paper quality and can be supposed to be given.

The system of equations describing the second phase reads:

$$\begin{aligned} E_1(\varepsilon_1) + \Lambda_1 c \frac{d}{dx} E_1(\varepsilon_1) - K\tau_{max} &= 0, \\ E_i(\varepsilon_i) + \Lambda_i c \frac{d}{dx} E_i(\varepsilon_i) &= 0, \qquad i = 2, \ldots, n. \end{aligned} \tag{19}$$

The values of $\varepsilon_i(x_r)$ are used as initial conditions. Equations (19) are similar to previous set of equations of *Phase 1* besides the fact that τ is zero. The solution of this system is given analytically by

$$\begin{aligned} E_1(\varepsilon_1(x)) &= C_1 \cdot e^{-\frac{x-x_r}{\Lambda_1 c}} + C_2, \\ E_i(\varepsilon_i(x)) &= E_i(\varepsilon_i(x_r)) \cdot e^{-\frac{x-x_r}{\Lambda_i c}}, \qquad i = 2, \ldots, n, \end{aligned}$$

where $C_1 = E_1(\varepsilon_1(x_r)) - K\tau_{max}(x_r)$ and $C_2 = K\tau_{max}(x_r)$. Now, we can calculate the input data needed by the flow solver. The porosity of each layer is computed by formula (6). The deformed grid which the flow solver needs is constructed from a regular mesh whose nodes are displaced (see Figure 7). More precisely, we store the z coordinates of points on $\Gamma_{b,i} \cup \Gamma_{b,c} \cup \Gamma_{b,o}$ during the elasticity computation. Since the step size of the Runge-Kutta method is much finer than the required mesh for the flow solver, we have precise information on the z coordinates of the flow mesh points on this boundary. Using the computed strains which are constant on each layer, the displacement of the flow mesh is immediately obtained. To obtain the solid velocities, we consider three points P_1, P_2 and P_3 as shown in Figure 7. Since the deformed mesh is still equidistant in machine direction, the x component of the solid velocity is set to machine speed. Hence, the time and the vertical distance to move from point P_1 to P_3 is known. We use this information to compute the solid velocity at P_2.

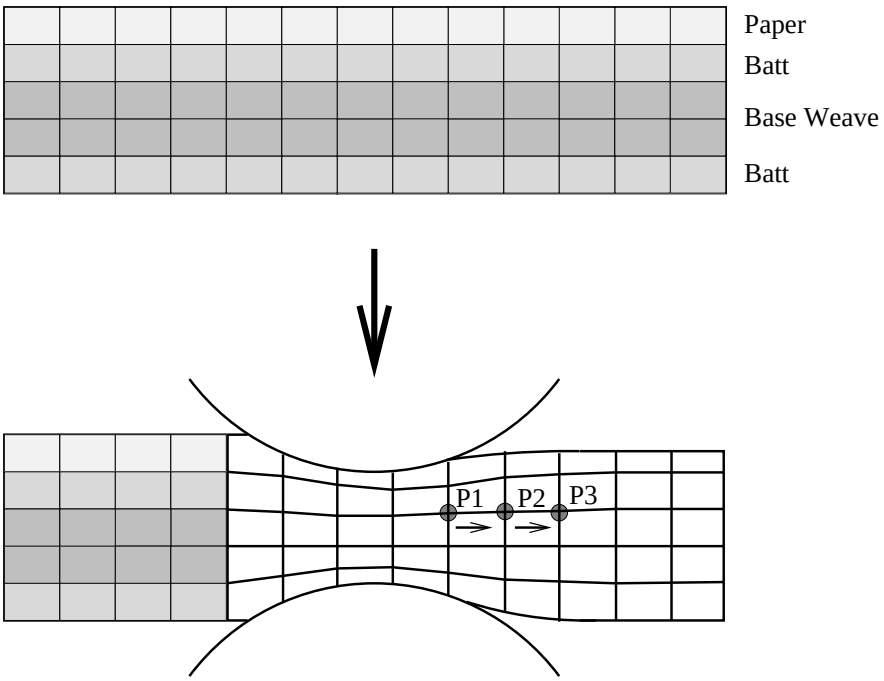

Figure 7: Regular and deformed mesh

3.2 Flow solver

The *design* of the algorithm to solve the flow problem (15) is guided by several observations. Since the flow problem is nonlinear, a suitable linearization has to be developed. The linearization induces some kind of iteration, whose convergence is strongly dependent on the initial choice of the solution. Remembering the boundary conditions for the pressure p_f, we immediately see, that p_f is equal to the constant Dirichlet boundary value on Γ_i, if the solid velocity is equal to zero. On the other hand, if the solid velocity increases, the pressure will rise, too. Therefore, as shown in Figure 6, a outer loop is implemented which increases the solid velocity. More precisely, starting from the known constant pressure solution, the solid velocity is scaled by a factor less than one and sufficiently small such that the nonlinear flow iteration steps (inner loop) converge. The scaling factor of the solid velocity is then increased and the inner loop is processed again. The iteration stops, when the desired final solid velocity is reached or other stopping criteria apply.

Let's have a closer look at the inner loop. We define

$$S' := \frac{\partial S(p_f)}{\partial p_f}.$$

Then, the truncated Taylor series of the retention function reads

$$S(p_f^{j+1}) \approx S(p_f^j) + S'(p_f^j)(p_f^{j+1} - p_f^j), \tag{20}$$

where $j \in \mathbb{N}$ is used as iteration index and p_f^{j+1} and p_f^j can be thought of two consecutive solutions of an iteration process. Plugging (20) into (15) and by further iterative linearization, we obtain

$$\begin{aligned} -\operatorname{div}\left(\left(S(p_f^j) + S'(p_f^j)(p_f^{j+1} - p_f^j)\right)\Phi \mathbf{v}_s\right) - \operatorname{div} \mathcal{F}_0^{\mathrm{nl}}(\nabla p_f^j, \Phi) \\ = -\operatorname{div}\left(\tfrac{\mathbf{K}_f^0}{\mu_f}\tfrac{\Phi^3}{1-\Phi^2}\, S(p_f^j)^b \cdot \nabla p_f^{j+1}\right). \end{aligned} \tag{21}$$

Reordering in terms of p_f^j and p_f^{j+1} yields

$$\begin{aligned} -\operatorname{div}\left(\left(S(p_f^j) - S'(p_f^j)p_f^j\right)\Phi \mathbf{v}_s\right) - \operatorname{div} \mathcal{F}_0^{\mathrm{nl}}(\nabla p_f^j, \Phi) \\ = -\operatorname{div}\left(\tfrac{\mathbf{K}_f^0}{\mu_f}\tfrac{\Phi^3}{1-\Phi^2}\, S(p_f^j)^b \cdot \nabla p_f^{j+1} - S'(p_f^j)p_f^{j+1}\Phi \mathbf{v}_s\right). \end{aligned} \tag{22}$$

Remark 2 The linearization of (15) is motivated by Newton-type methods. Numerical experiments show that the expansion (20) is quite important to guaranty fast convergence.

In view of a finite element discretization of (22), a variational formulation is derived. Due to the Dirichlet boundary conditions on Γ_i, we define a subspace of $H^1(\Omega)$ by

$$V := \{v \in H^1(\Omega) \mid v = 0 \quad \text{on } \Gamma_i\},$$

where the domain Ω is the union of all deformed layers $\Omega_1, \ldots, \Omega_n$ (see Figure 4). The pressure can be decomposed into

$$p_f^j = \hat{p}_f^j + p_0, \quad \hat{p}_f^j \in V \text{ and } p_0 \in H^1(\Omega), \tag{23}$$

where the function p_0 (as extension of a constant function on Γ_i into $H^1(\Omega)$) represents the Dirichlet conditions on Γ_i.
Now, let $w \in V$ be a test function. Multiplying (22) by w, using (23),

integrating over Ω and applying Green's formula , yields

$$
\begin{aligned}
&\int_\Omega \left(\left(S(p_f^j) - S'(p_f^j) p_f^j \right) \Phi \mathbf{v}_s + \mathcal{F}_0^{\mathrm{nl}}(\nabla p_f^j, \Phi) \right) \cdot \nabla w \, dx \qquad (24)\\
&- \int_{\partial\Omega} \nu(x) \cdot \left(\left(S(p_f^j) - S'(p_f^j) p_f^j \right) \Phi \mathbf{v}_s + \mathcal{F}_0^{\mathrm{nl}}(\nabla p_f^j, \Phi) \right) w \, d\Gamma(x)\\
&- \int_\Omega \left(\frac{\mathbf{K}_f^0}{\mu_f} \frac{\Phi^3}{1-\Phi^2} S(p_f^j)^b \cdot \nabla p_0 - S'(p_f^j) p_0 \Phi \mathbf{v}_s \right) \cdot \nabla w \, dx\\
&+ \int_{\partial\Omega} \nu(x) \cdot \left(\frac{\mathbf{K}_f^0}{\mu_f} \frac{\Phi^3}{1-\Phi^2} S(p_f^j)^b \cdot \nabla p_0 - S'(p_f^j) p_0 \Phi \mathbf{v}_s \right) w \, d\Gamma(x)\\
= &\int_\Omega \left(\frac{\mathbf{K}_f^0}{\mu_f} \frac{\Phi^3}{1-\Phi^2} S(p_f^j)^b \cdot \nabla \hat{p}_f^{j+1} - S'(p_f^j) \hat{p}_f^{j+1} \Phi \mathbf{v}_s \right) \cdot \nabla w \, dx\\
&- \int_{\partial\Omega} \nu(x) \cdot \left(\frac{\mathbf{K}_f^0}{\mu_f} \frac{\Phi^3}{1-\Phi^2} S(p_f^j)^b \cdot \nabla \hat{p}_f^{j+1} - S'(p_f^j) \hat{p}_f^{j+1} \Phi \mathbf{v}_s \right) w \, d\Gamma(x).
\end{aligned}
$$

In (24), all boundary integrals vanish due to the specified boundary conditions and due to the properties of the test function. Hence, we have the following variational formulation:

$$
\begin{aligned}
&\text{Find } \hat{p}_f^{j+1} \in V, \text{such that} \qquad (25)\\
&\int_\Omega \left(\left(S(p_f^j) - S'(p_f^j) p_f^j \right) \Phi \mathbf{v}_s + \mathcal{F}_0^{\mathrm{nl}}(\nabla p_f^j, \Phi) \right) \cdot \nabla w \, dx\\
&- \int_\Omega \left(\tfrac{\mathbf{K}_f^0}{\mu_f} \tfrac{\Phi^3}{1-\Phi^2} S(p_f^j)^b \cdot \nabla p_0 - S'(p_f^j) p_0 \Phi \mathbf{v}_s \right) \cdot \nabla w \, dx\\
= &\int_\Omega \left(\tfrac{\mathbf{K}_f^0}{\mu_f} \tfrac{\Phi^3}{1-\Phi^2} S(p_f^j)^b \cdot \nabla \hat{p}_f^{j+1} - S'(p_f^j) \hat{p}_f^{j+1} \Phi \mathbf{v}_s \right) \cdot \nabla w \, dx, \quad \forall w \in V.
\end{aligned}
$$

As already mentioned above, at least for moderate solid velocities, (25) is an elliptic problem. It is solved by a finite element discretization. The pressure is discretized by bilinear Ansatz functions on quadrilateral grids. Matrix assembly is done on a reference element using the nine-point Gaussian integration rule. Due to the deformation, we have to handle general quadrilaterals. Therefore, the simple coordinate transformation of the square case has to be extended. We used a standard method for which we refer to [10], p. 188ff. The system of linear equations is directly solved by SuperLU 3.0 (see [6]).

4 General model parameters

The aim of this section is to provide model parameters for the numerical studies at the end of this chapter. To determine the permeability tensor $\mathbf{K}_f^0$, we create a virtual felt made of three layers. Inspired by images like

the one shown in Figure 8 and data from [13], the virtual felt has a fine fiber batt layer on top, a base weave in the middle and, finally, another batt layer.

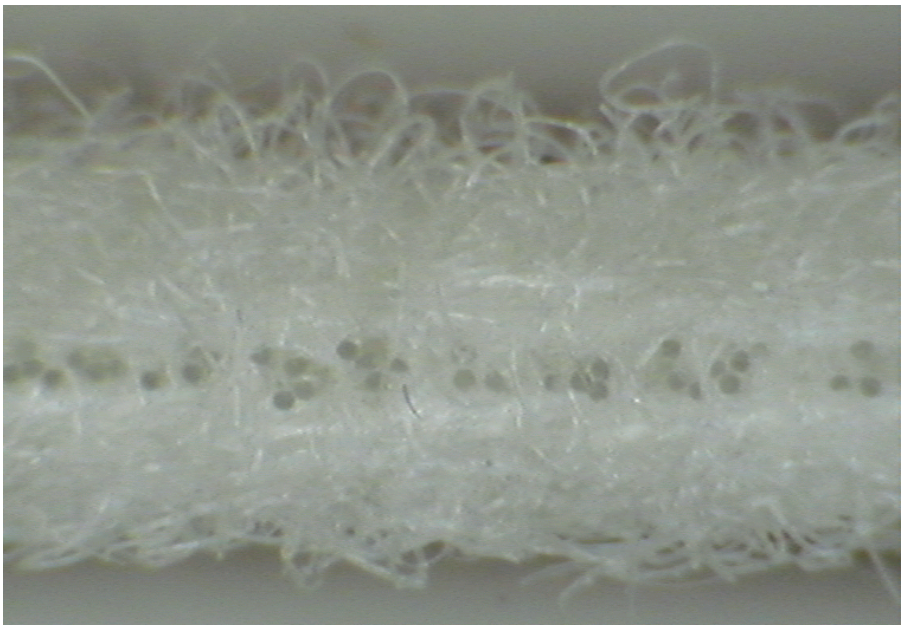

Figure 8: Cross section of a dewatering felt

The upper batt layer has a length of 1 mm in the transversal direction and its porosity is 60 %. It consists of 50 % 10 dtex and 50 % 20 dtex fibers made from polyamid 6. The unit *dtex* is equivalent to 1 g / 10000 m and, hence, the actual diameter depends on the material's density. In case of polyamid 6 and round fibers, 10 dtex and 20 dtex correspond to 33.4 μm and 47.3 μm, respectively. The other batt layer has a thickness of 0.5 mm, 20 dtex fibers only, and its porosity is 65 %. The base weave has a certain arrangement of yarns. Each yarn is 350 μm thick. We added a mixture of 50 % 10 dtex and 50 % 20 dtex fibers, which then results in an overall porosity of 45 %. The thickness is 1.5 mm. Since the fibers are usually attached to the base weave by a needling process, the fiber orientation is chosen to be transversally dominated. Figures 9, 10, 11 illustrate the generated geometries. All layers are created by GeoDict, which is a virtual structure generator developed at Fraunhofer ITWM. The resolution is chosen to be 5 μm. The lateral cross section of each layer is 1.8×1.8 mm^2.

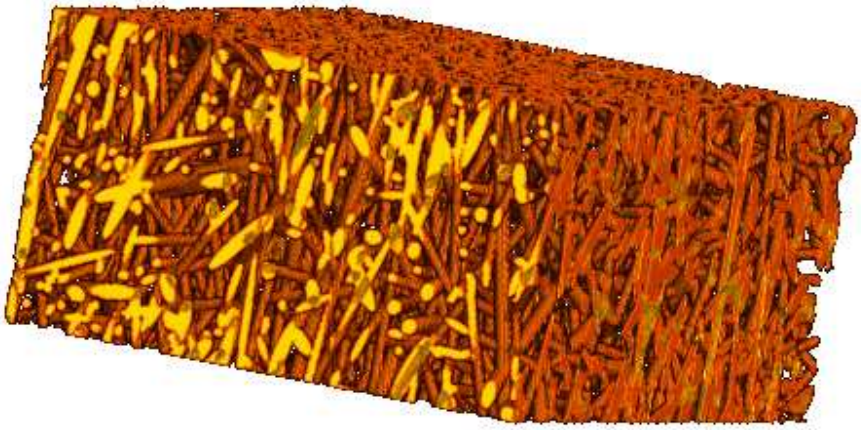

Figure 9: Model of the upper batt fiber layer

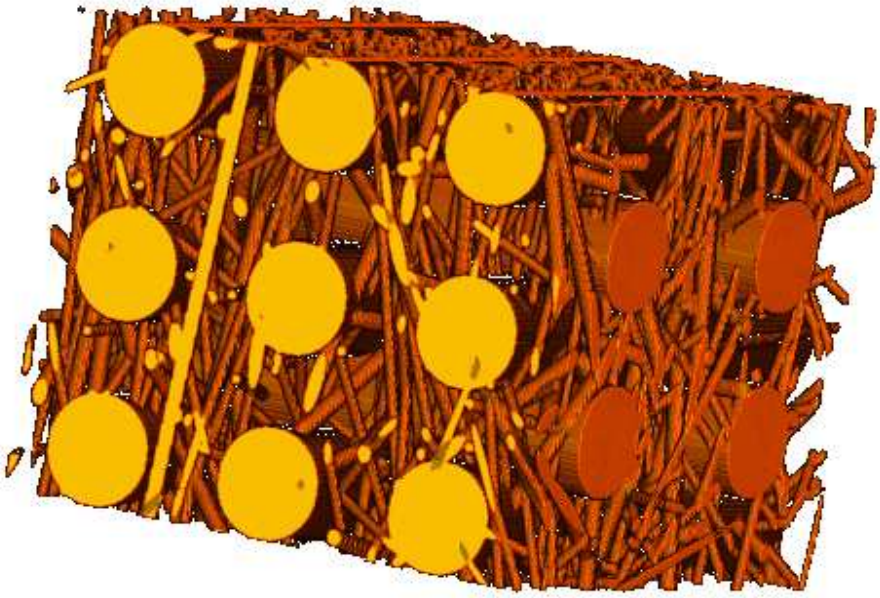

Figure 10: Model of the base weave layer

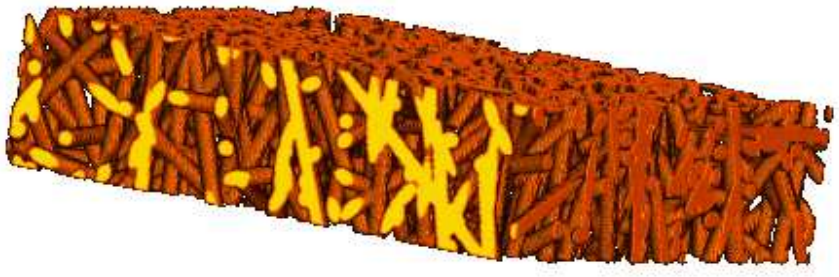

Figure 11: Model of the lower batt fiber layer

By the use of ParPac, which is a lattice Boltzmann solver by Fraunhofer ITWM, we can compute the permeability tensor $\mathbf{K}_f^0$ of the individual layers in three dimensions. More precisely, Stokes problems are calculated quite similar to the cell problems introduced in Chapter 2 of [11]. The only difference is, that we don't homogenize the Stokes system, but calculate the effective permeability, i.e. essentially a velocity-pressure-drop relation on a sufficiently large volume element of the porous medium, i.e. of the felt. The calculated permeabilities restricted to the x- and z-direction are shown in Table 1. Due to the computational complexity, we can not compute nonlinear filtration laws as done in Chapter 3 of [11]. However, simulations indicate that nonlinear effects are important. At pressure drops of 10000 Pa/mm applied to the layers, one observes flow rates being significantly smaller than in the linear case. Motivated by these observations , we construct nonlinear filtration laws, which give at least qualitatively the correct behavior and allow to study the influence of inertia on paper dewatering. Based on a linear interpolation of the computed data given in Table 2, we determine $\mathcal{F}_0^{nl}$. For simplicity, we drop the dependence on the porosity.
Additional parameters of the elasticity and fluid dynamical model are based on data given in [14]: For each layer, we set the residual saturation to be $s_\infty = 0.1$. The shape factor b in (11) is chosen to be 3.4 and the fluid pressure at the inlet is $p_{f|\Gamma_i} = -5000$ Pa. For the dynamic viscosity we assume $\mu_f = 6.53 * 10^{-4}$ Pa s. This value corresponds to water viscosity at 40 ℃. The initial saturations are 0.55, 0.45 and 0.50 for upper batt, base weave and lower batt, respectively. In [14] measurements to determine the viscoelastic parameters of an entire felt are presented. The stress-strain relation is assumed nonlinear, i.e. $E(\varepsilon) = A \cdot \varepsilon^r$ and we obtain $r = 2$ and $A = 40$ MPa. The viscoelastic time constant λ is of size 0.4 ms. It can be expected, that the individual layers deform differently due to their different constituents. Therefore, we preserve the structure of the nonlinear law in each layer, but vary the constant A as listed in Table 1. Note, that the

	Upper Batt	Base	Lower Batt
l_0 [mm]	1.00	1.50	0.50
A [MPa]	30	70	40
r [1]	2	2	2
λ [ms]	0.4	0.4	0.4
Φ_0 [1]	0.60	0.45	0.65
S_0 [1]	0.55	0.45	0.50
$K^0_{f_{xx}}$ [m^2]	$8.77 * 10^{-11}$	$4.97 * 10^{-10}$	$1.73 * 10^{-10}$
$K^0_{f_{zz}}$ [m^2]	$1.54 * 10^{-10}$	$1.12 * 10^{-9}$	$2.50 * 10^{-10}$
$K^0_{f_{xz}} = K^0_{f_{zx}}$ [m^2]	$1.44 * 10^{-12}$	$8.57 * 10^{-12}$	$-5.34 * 10^{-12}$

Table 1: Felt parameters

	Upper Batt	Base	Lower Batt
MD-Ratio at 1 Pa/mm [%]	100.0	100.0	100.0
MD-Ratio at 2000 Pa/mm [%]	95.0	68.0	81.0
MD-Ratio at 10000 Pa/mm [%]	72.0	40.0	51.0
CD-Ratio at 1 Pa/mm [%]	100.0	100.0	100.0
CD-Ratio at 2000 Pa/mm [%]	93.0	70.0	78.0
CD-Ratio at 10000 Pa/mm [%]	70.0	40.0	48.0

Table 2: Computed ratios of nonlinear and linear flow rates in MD and CD

overall elastic response is not preserved by this heuristic choice. However, we are only interested to have qualitatively reasonable parameters, which are in the range of existing felt designs.

Now, we discuss the parameters of the paper layer, roll surface and belt. Due to the lack of measurements, the elastic parameters of the paper layer are chosen to give reasonable deformation during pressing. We want to observe a *gradual* deformation of the paper and its thickness should be decreased by not more than 50 %. Due to fine cellulose fibers, which are in the range of 10 μm, the paper permeability is set lower than the felt permeability. Test simulations in a micro structure made of 10 μm fibers give permeabilities, which are one up to two orders smaller than the felt permeabilities. Moreover, it is well-known that the orientation of paper fibers is aligned to the machine direction due to process conditions in the forming section. We account for it by introducing an anisotropy of the permeability values in

	Paper	Roll surface	Belt
l_0 [mm]	0.3	3	3
A [MPa]	40	10000	10000
r [1]	1.6	1	1
λ [ms]	0.4	0.4	0.4
K [1]	0.7	–	–
Φ_0 [1]	0.7	0.25	0.25
S_0 [1]	0.99	0.4 | 0.6	0.4 | 0.6
$K^0_{f_{xx}}$ [m^2]	$1.0 * 10^{-11}$	$1.0 * 10^{-8}$	$1.0 * 10^{-8}$
$K^0_{f_{zz}}$ [m^2]	$6.0 * 10^{-12}$	$1.0 * 10^{-8}$	$1.0 * 10^{-8}$
$K^0_{f_{xz}} = K^0_{f_{zx}}$ [m^2]	0.0	0.0	0.0

Table 3: Parameters of paper, roll surface and belt

x- and z-direction. Again, the ratio is determined by simulations using the micro structure made of 10 μm fibers. To account for inertia, the nonlinear filtration law of the paper layer is chosen similarly as in the case of the upper batt fiber layer. The *dry solids content* of paper is typically defined by the ratio of fiber mass to total mass. The initial saturation and initial porosity are chosen such that the dry solids content is 27.8 % assuming a paper weight of 80 g/m^2 . In our numerical studies, the roll surfaces and belts possess wholes and a grooved structure, respectively. The dimension of the wholes and grooves are in the range of millimeters. Therefore, we chose a rather large permeability. Moreover, these layers will never be fully saturated in our simulation, which makes the use of nonlinear filtration laws obsolete. The elastic stiffness is relatively large compared to the fibrous structures. Hence, small deformations can be expected and it is reasonable to assume linear behavior. Typical values of A are in the range of 10000 MPa. The initial saturation are set to either 40 % or 60 %. All parameters are listed in Table 3.

Two types of press configurations are considered in the following section. The first type is a roll press nip. The rolls are 1200 mm in diameter and positioned at $x = 0$ mm. The second type is a shoe press nip. The shoe is modeled as part of a circle with radius 1000 mm being positioned at $x = 0$ mm. The length of the shoe is chosen to be 250 mm. The opposing roll has a radius of 900 mm and its center is positioned at $x = 3$ mm. The arrangement of the layers is as follows: On top, there is the paper layer. Then, the three felt layers, i.e. upper batt, base weave and lower batt, follow. In case of the roll press nip, we find the roll surface as the lowest layer. In case of the shoe press nip, the final layer is formed by the belt.

As indicated by Figure 3, the paper layer is separated from the felt right after the press nip. Therefore, we introduce one paper separation point at $x = 40$ mm and $x = 140$ mm in case of the roll press nip and the shoe press nip, respectively. At the specific point, a boundary is introduced between the paper layer and the upper batt layer, which reaches to the right boundary of the computational domain and suppresses any fluid flow. Analogously, separating boundaries for the roll surface and the belt are introduced. They are determined by x_r and x_l (see Figure 4).

5 Numerical results and discussion

We use the parameters of the previous section unless otherwise stated. All numerical examples are discretized by a 1500×500 mesh. In case of the roll press, we simulate the nip for $x \in [-100, 400]$. The shoe press simulations are done in the range of $x \in [-300, 400]$. We start the computations at $\mathbf{v}_s = 250$ m/min and increase the solid velocity in steps of 250 m/min. At each velocity level, we solve the nonlinear problem until the relative accuracy of the pressure update is less than 10^{-4}. To reach this precision, typically five up to ten iterations are needed.

5.1 Roll press nip

In this section, we present numerical results of a roll press nip. The minimum distance d_{min} of the press profiles is automatically adjusted to match a press force of 200 kN/m. In Figure 12, 13, the porosity is shown at $\mathbf{v}_s = 750$ m/min and $\mathbf{v}_s = 1250$ m/min, respectively. Higher machine speeds increase viscoelastic stresses, hence the permanent deformation of the paper layer becomes larger. Note, that the roll surface is hardly compressed in this setting.
Now, we consider results related to the flow model without nonlinear filtration laws. The degree of saturation is presented in Figure 14, 15 and 16. Figure 14 corresponds to $\mathbf{v}_s = 750$ m/min and an initial saturation of the roll surface of 40 %. In Figure 15, the machine speed is increased to $\mathbf{v}_s = 1250$ m/min. Additionally, in Figure 16, the initial saturation of the roll surface is set to 60 %, which shows a strong effect building up a fully saturated zone in transversal direction. All pictures show how the fluid is transported from the paper through the felt entering the roll surface.
For the same three setting, the hydrodynamic pressure is shown in Figure 17, 18 and 19. Due to the stronger compression especially of the paper layer, a larger amount of fluid has to be transported in shorter time and, therefore, the pressure increases as the machine speed goes up. In Figure 19, this effect becomes even stronger which is due to the increased fluid content of the roll surface.

In Figure 20, the fluid velocity is illustrated. The dewatering zone right before the center of the nip can clearly be observed. The dewatering turns into rewetting, which is less obvious, but very important in practice. Looking at Figure 21, a typical profile of the dry solids content of paper is plotted. Here, the dewatering and rewetting zones are clearly observable. The final dry solids contents of the paper layer are 41.80 %, 43.11 % and 41.47 % for the three settings, respectively. This result is consistent with the aforementioned remarks on compression and fluid content of the overall nip.
Finally, we investigate the effect of inertia. Figure 22 corresponds to Figure 14. The saturations hardly differ. However, the underlying model included nonlinear filtration laws. The situation changes when looking at the pressures. Corresponding to Figure 17, 18 and 19, we see in Figure 23, 24 and 25 significantly increased hydrodynamic pressures.
From this observations, we draw the following conclusions: Since the saturations hardly change when incorporating nonlinear filtration laws in the flow model, the dewatering performance of the nip is hardly effected. Nevertheless, looking at Figure 26 and thinking of higher machine speeds, it might be reasonable to consider hydrodynamic pressures as additional stress in the elasticity model. This will increase d_{min} and influence the flow problem via changes in porosity.

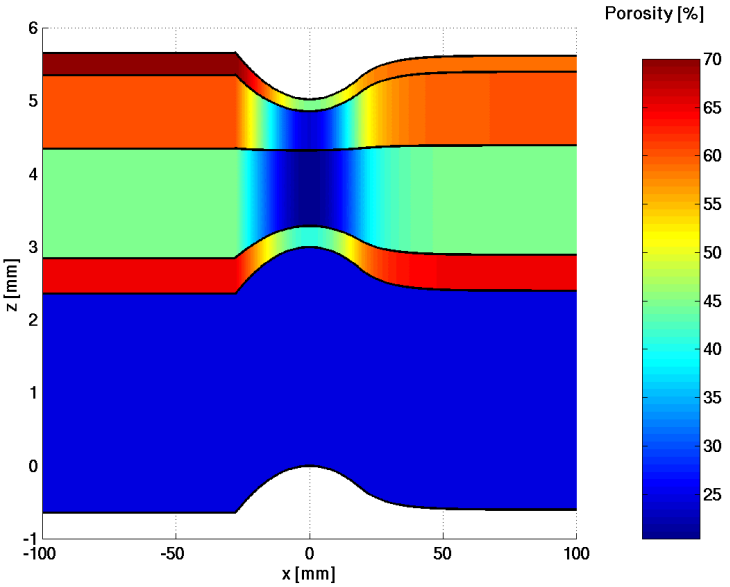

Figure 12: Porosity: $\mathbf{v}_s = 750$ m/min

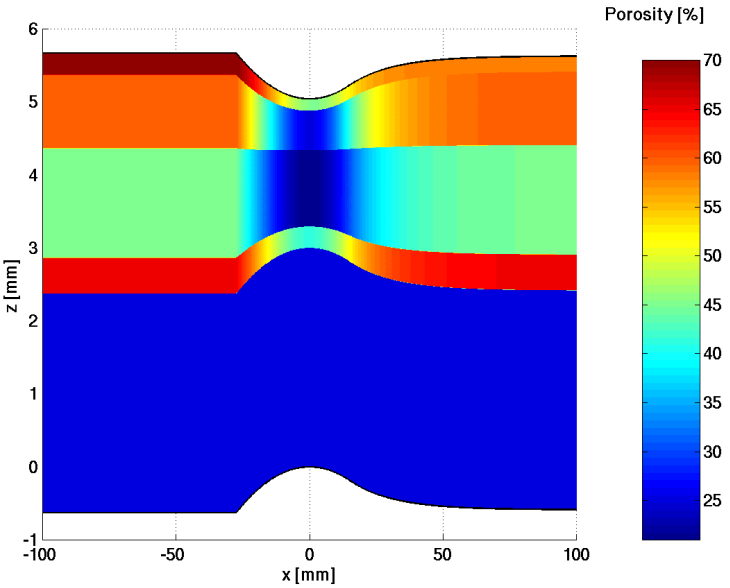

Figure 13: Porosity: $\mathbf{v}_s = 1250$ m/min

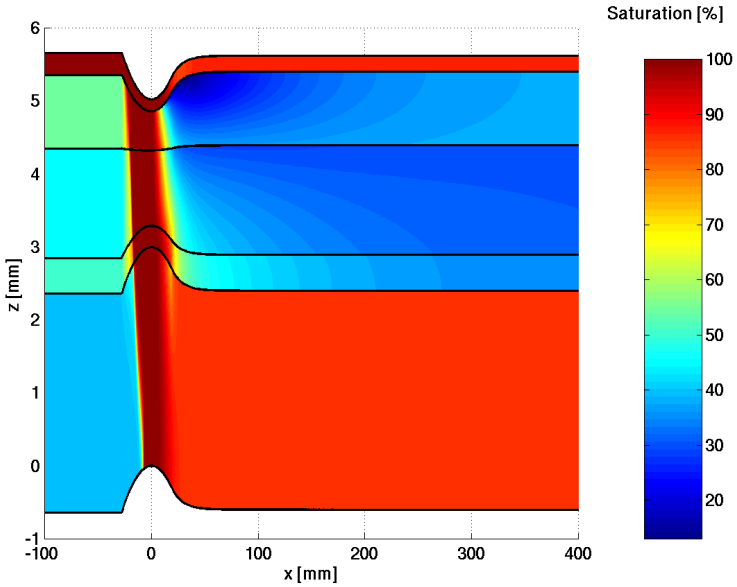

Figure 14: Saturation: $\mathbf{v}_s = 750$ m/min and initial roll surface saturation $S_0 = 40$ %

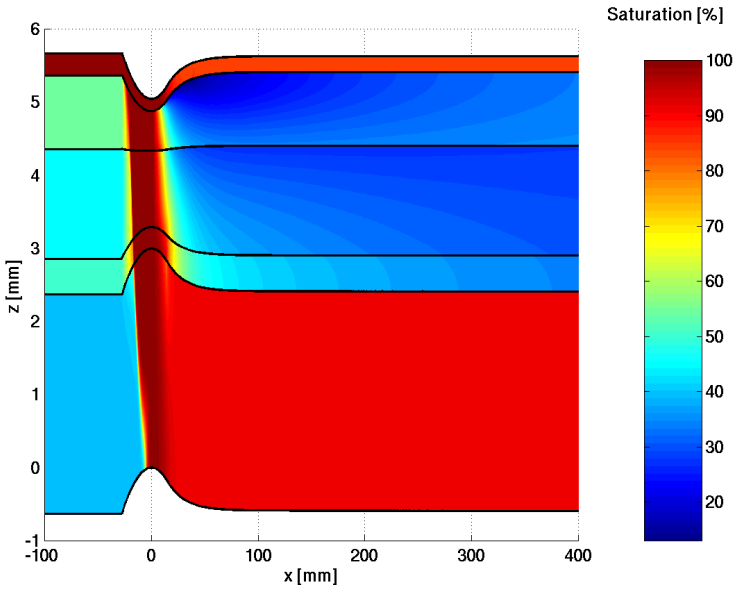

Figure 15: Saturation: $\mathbf{v}_s = 1250$ m/min and initial roll surface saturation $S_0 = 40$ %

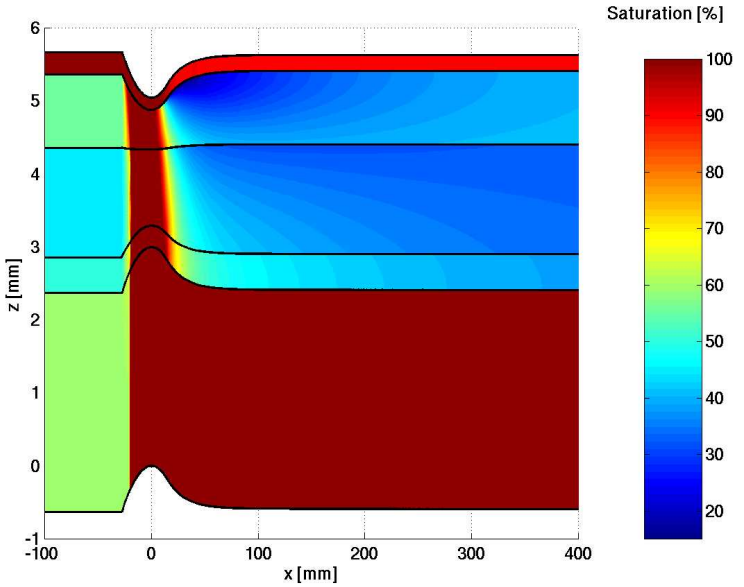

Figure 16: Saturation: $\mathbf{v}_s = 1250$ m/min and initial roll surface saturation $S_0 = 60$ %

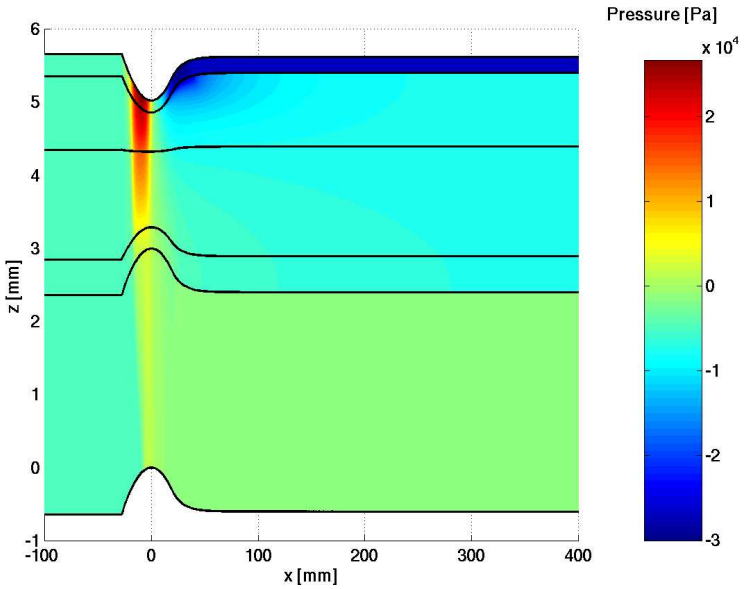

Figure 17: Pressure: $\mathbf{v}_s = 750$ m/min and initial roll surface saturation $S_0 = 40$ %

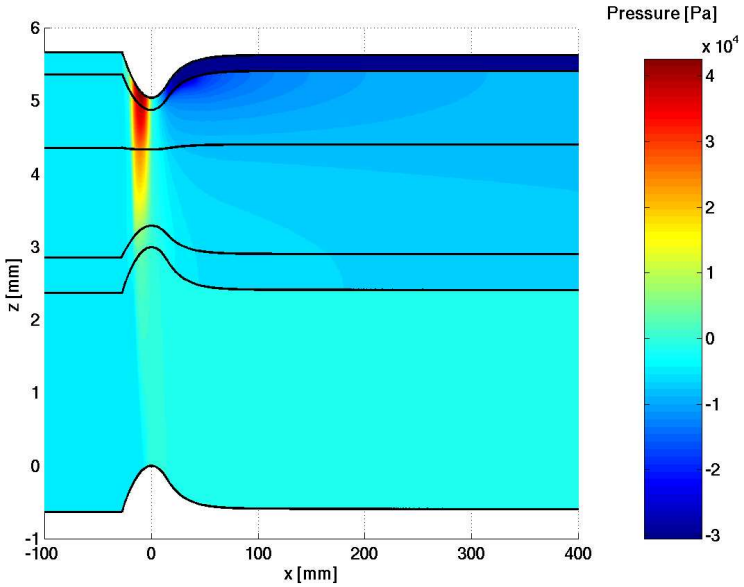

Figure 18: Pressure: $\mathbf{v}_s = 1250$ m/min and initial roll surface saturation $S_0 = 40$ %

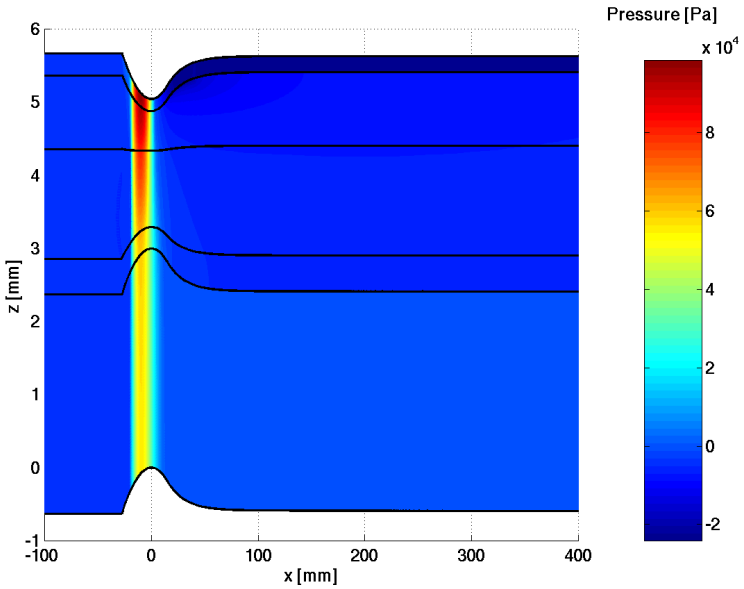

Figure 19: Pressure: $\mathbf{v}_s = 1250$ m/min and initial roll surface saturation $S_0 = 60$ %

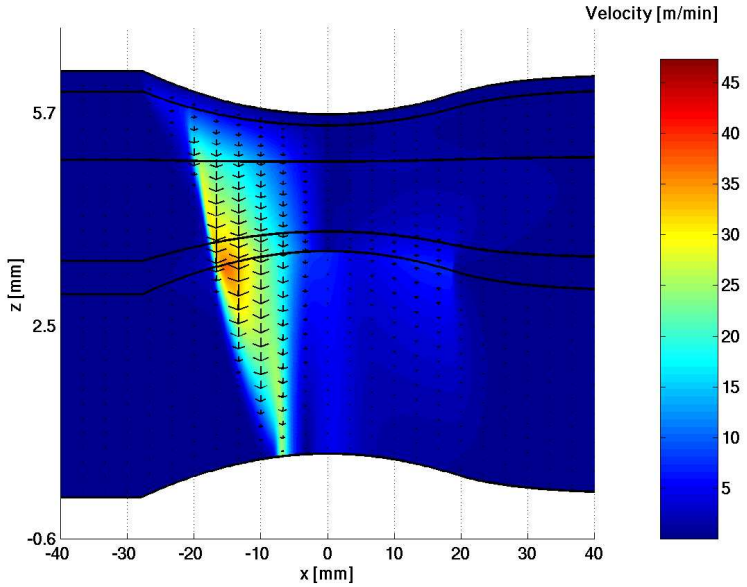

Figure 20: Velocity: $\mathbf{v}_s = 750$ m/min and initial roll surface saturation $S_0 = 40$ %

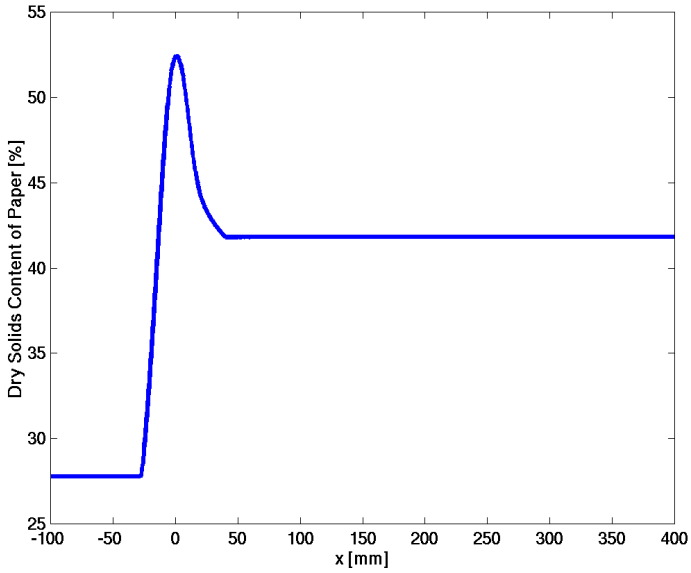

Figure 21: Typical profile of the dry solids content of paper

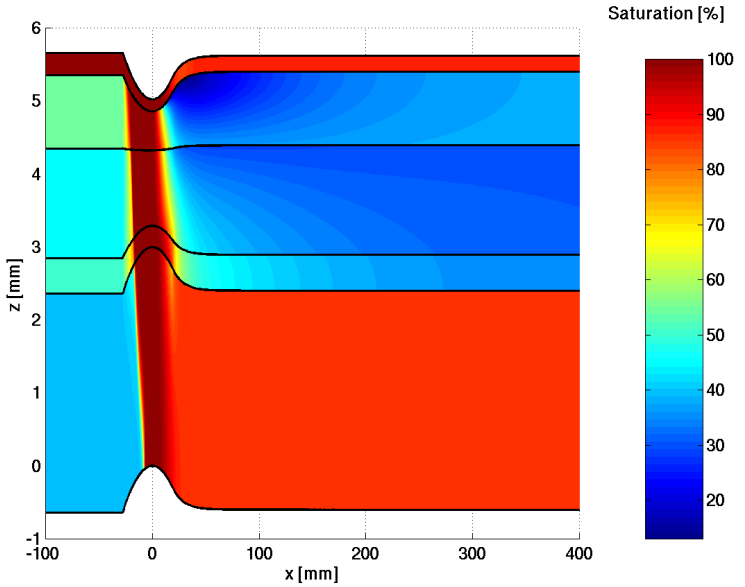

Figure 22: Saturation: $\mathbf{v}_s = 750$ m/min, initial roll surface saturation $S_0 = 40$ % and with inertia

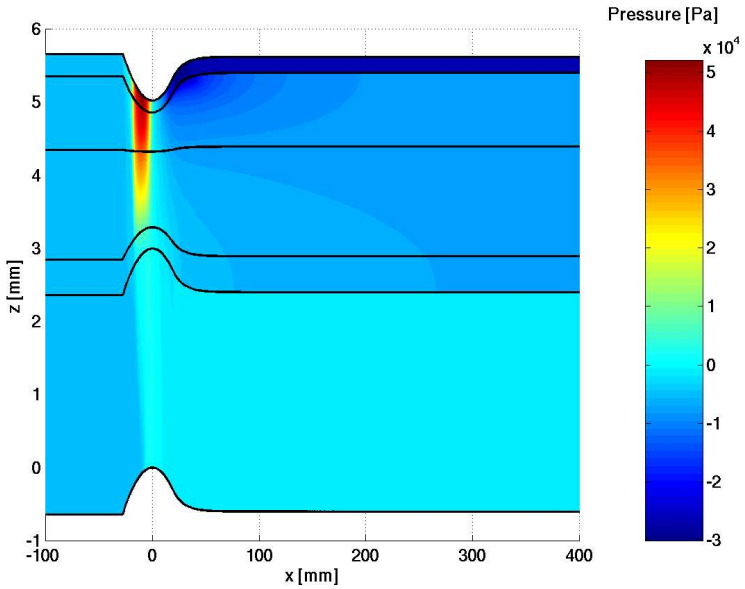

Figure 23: Pressure: $\mathbf{v}_s = 750$ m/min, initial roll surface saturation $S_0 = 40$ % and with inertia

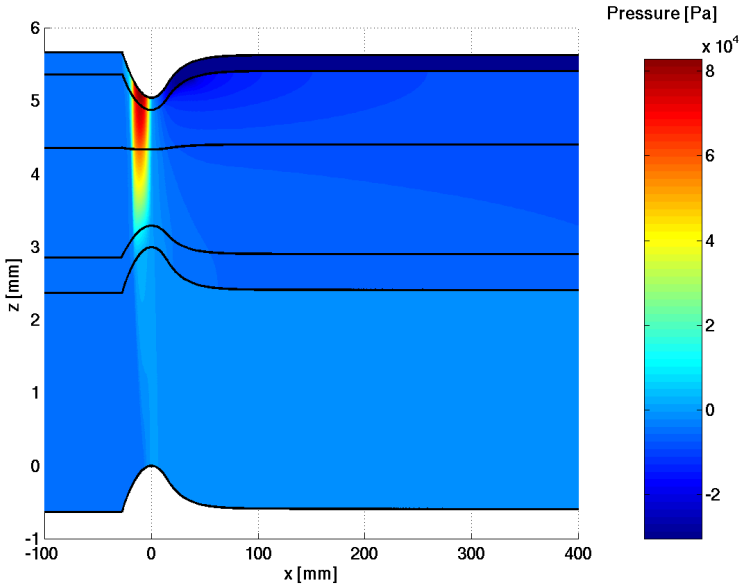

Figure 24: Pressure: $\mathbf{v}_s = 1250$ m/min, initial roll surface saturation $S_0 = 40$ % and with inertia

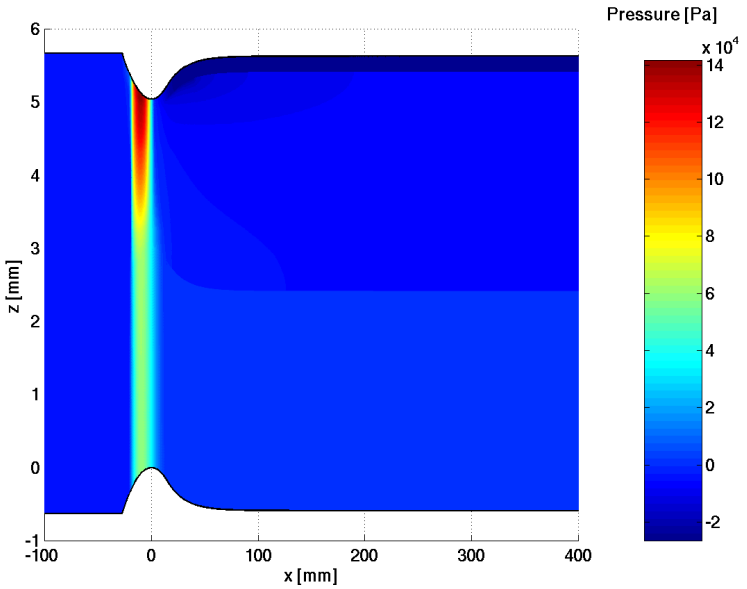

Figure 25: Pressure: $\mathbf{v}_s = 1250$ m/min, initial roll surface saturation $S_0 = 60$ % and with inertia

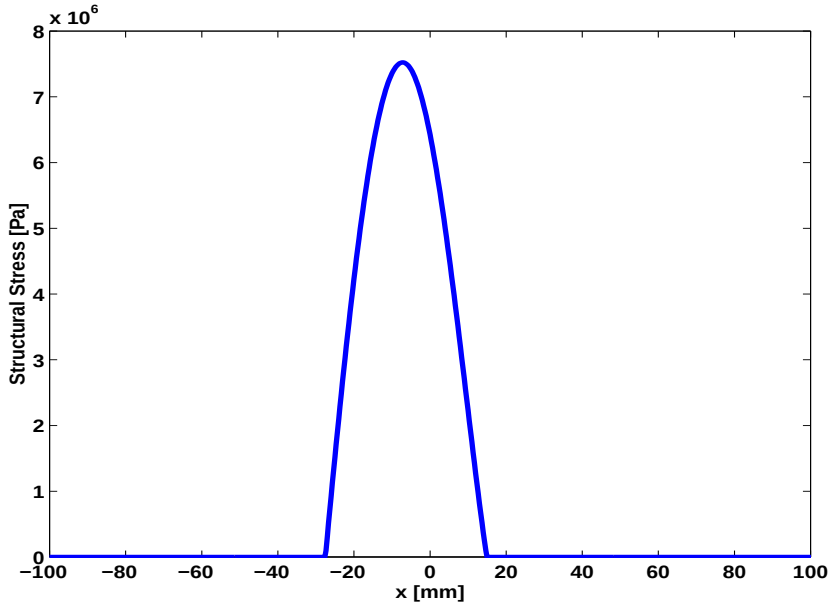

Figure 26: Structural stress: $\mathbf{v}_s = 750$ m/min

5.2 Shoe press nip

For the sake of completeness, we present simulation results of a shoe press nip. The behavior of the model is quite similar to the simulation results of the previous section. The minimum distance d_{min} of the press profiles is automatically adjusted to match a press force of 1100 kN/m. We consider three variations of the machine velocity and initial saturation of the belt, which replaced the roll surface of the roll press nip. The following sequence of figures is ordered as in the case of the roll press nip and similar comments hold. The final dry solids content at $\mathbf{v}_s = 750$ m/min and initial belt saturation of 40 % reads 39.95 %. Increasing the machine speed to $\mathbf{v}_s = 1100$ m/min yields 41.46 % dry solids content. Additionally setting the initial belt saturation to 60 % gives a dry solids content of 39.62 %.

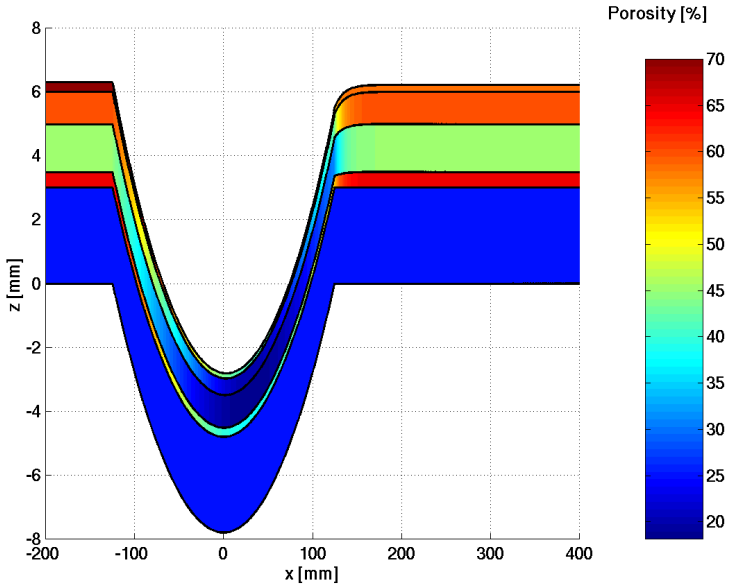

Figure 27: Porosity: $\mathbf{v}_s = 750$ m/min

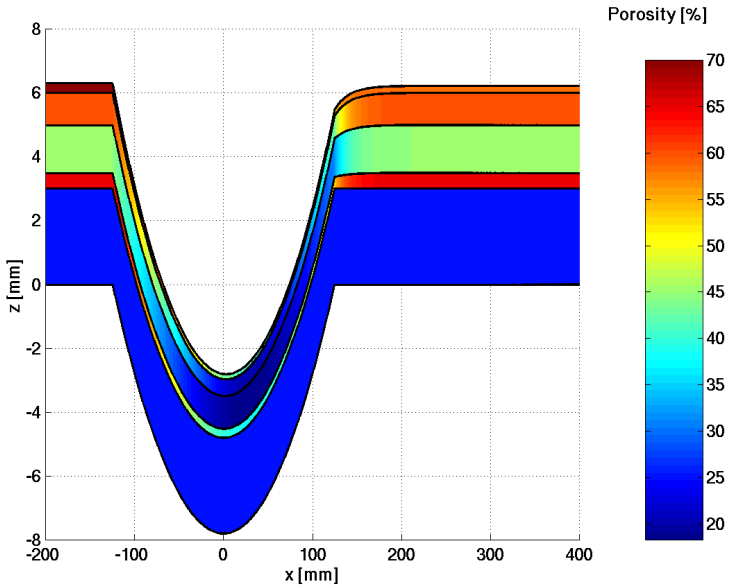

Figure 28: Porosity: $\mathbf{v}_s = 1250$ m/min

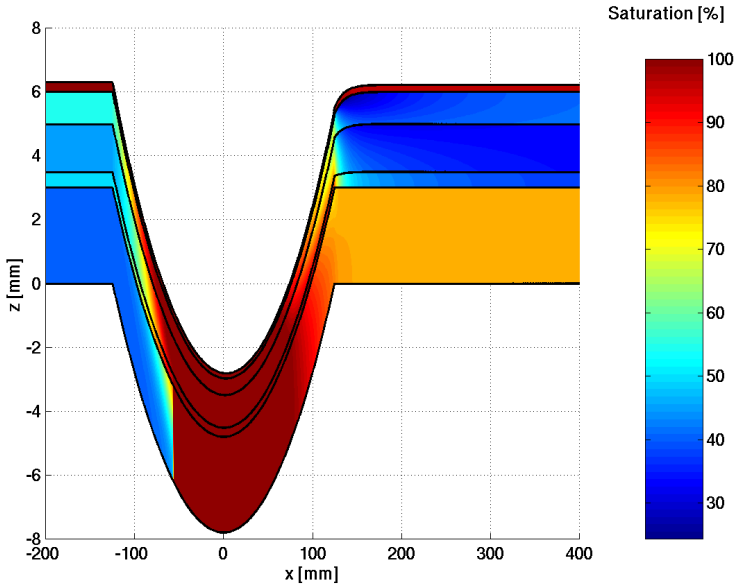

Figure 29: Saturation: $\mathbf{v}_s = 750$ m/min and initial belt saturation $S_0 = 40$ %

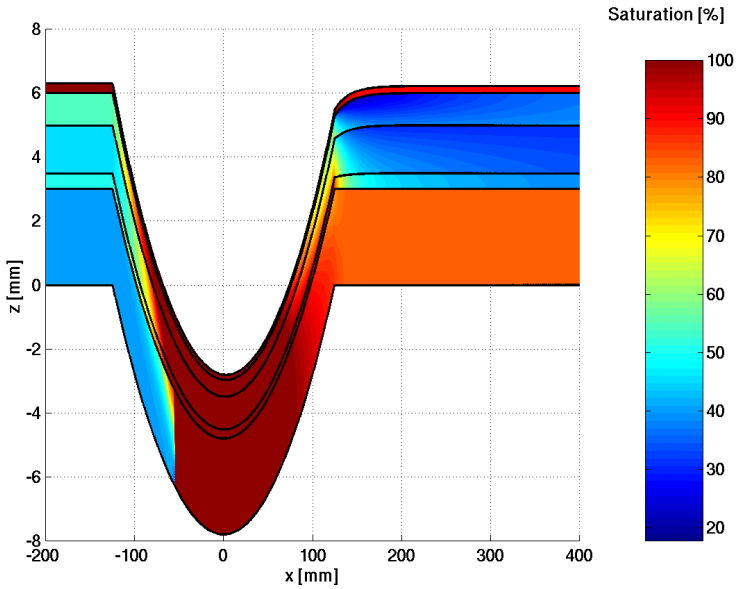

Figure 30: Saturation: $\mathbf{v}_s = 1250$ m/min and initial belt saturation $S_0 = 40$ %

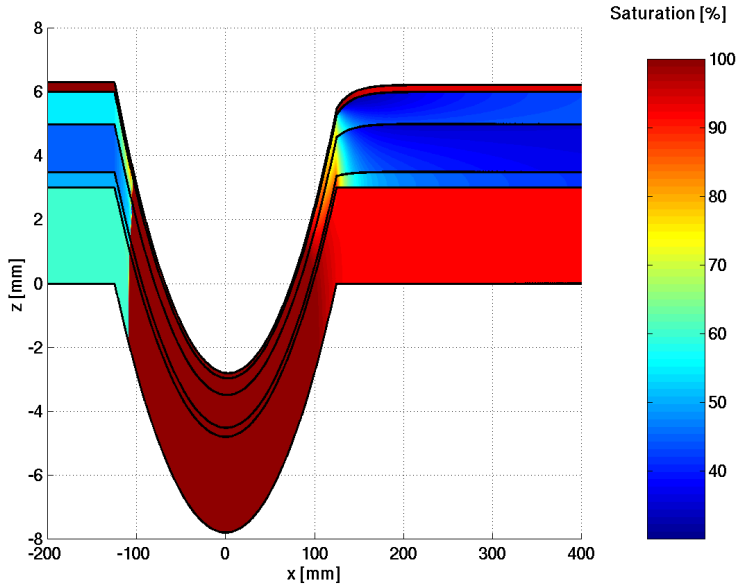

Figure 31: Saturation: $\mathbf{v}_s = 1250$ m/min and initial belt saturation $S_0 = 60$ %

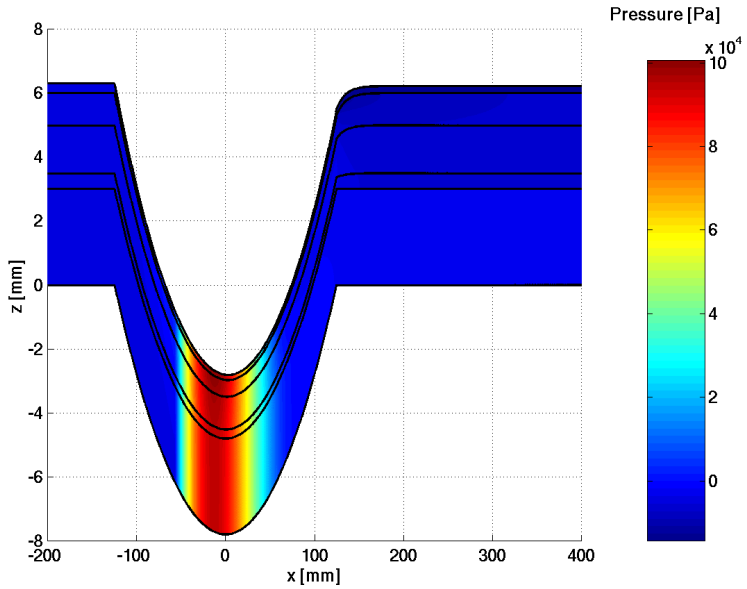

Figure 32: Pressure: $\mathbf{v}_s = 750$ m/min and initial belt saturation $S_0 = 40$ %

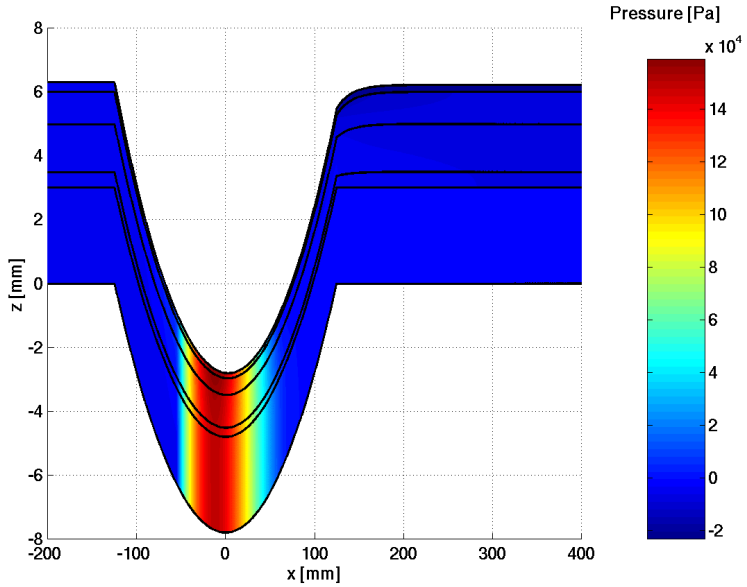

Figure 33: Pressure: $\mathbf{v}_s = 1250$ m/min and initial belt saturation $S_0 = 40$ %

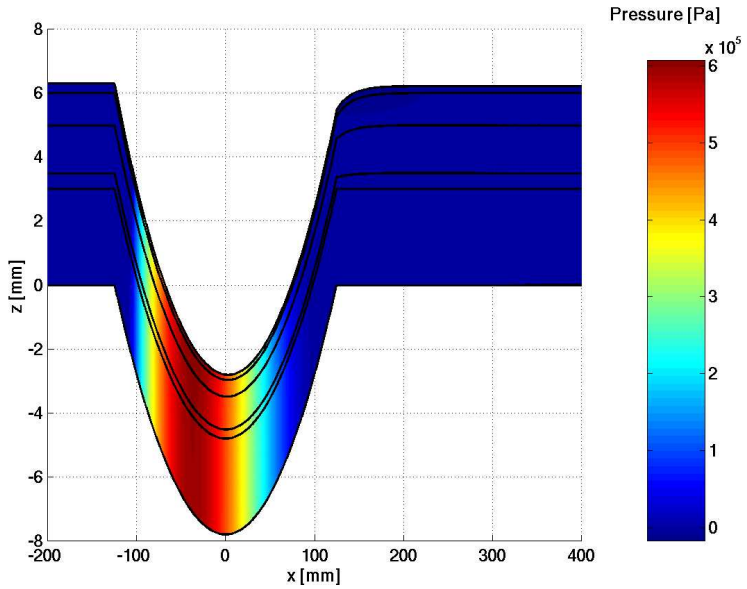

Figure 34: Pressure: $\mathbf{v}_s = 1250$ m/min and initial belt saturation $S_0 = 60$ %

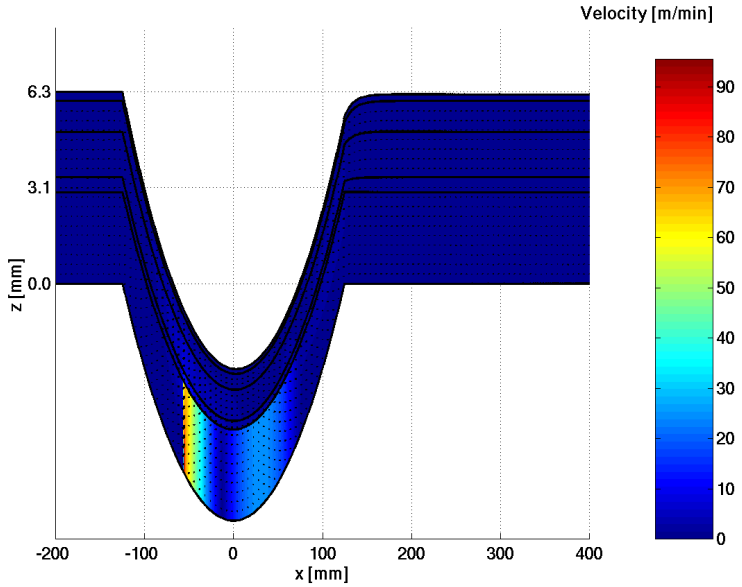

Figure 35: Velocity: $\mathbf{v}_s = 750$ m/min and initial belt saturation $S_0 = 40$ %

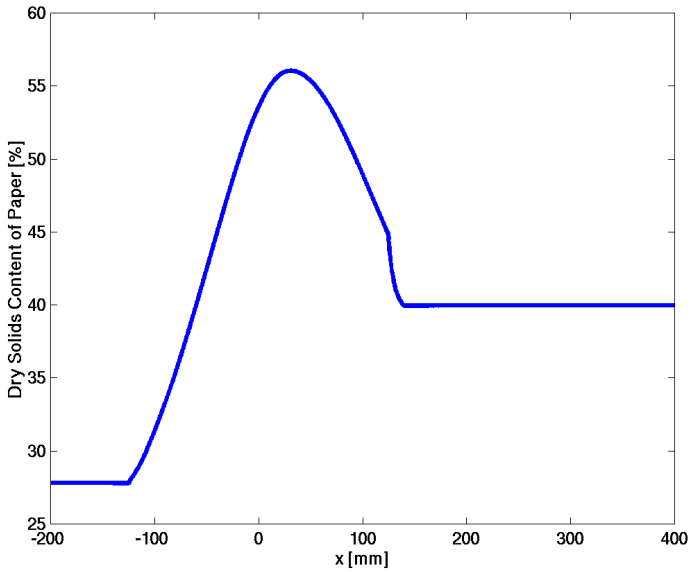

Figure 36: Typical profile of the dry solids content of paper

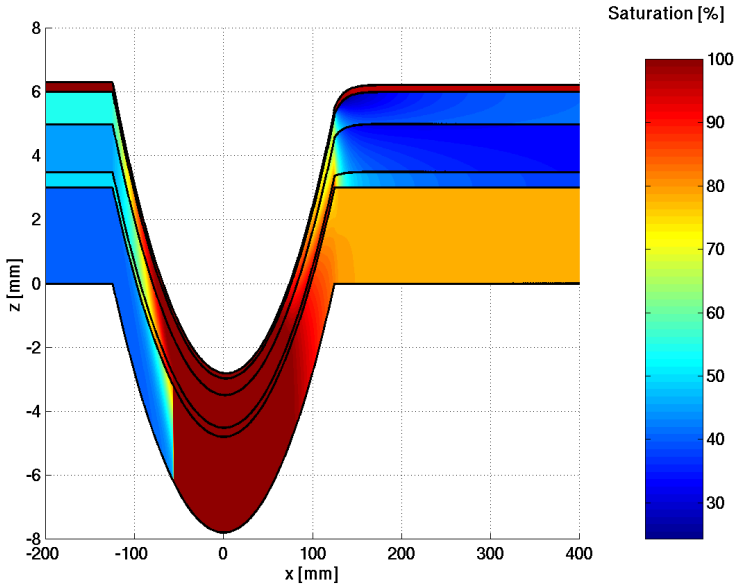

Figure 37: Saturation: $\mathbf{v}_s = 750$ m/min, initial belt saturation $S_0 = 40$ % and with inertia

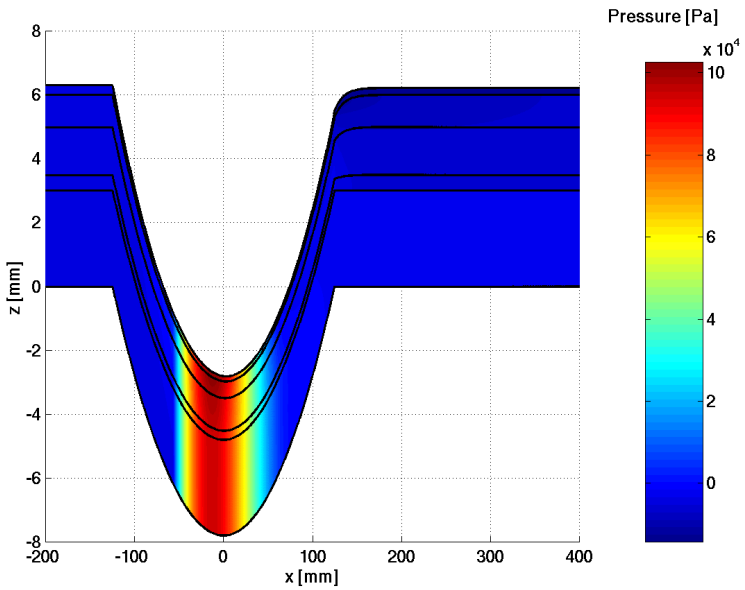

Figure 38: Pressure: $\mathbf{v}_s = 750$ m/min, initial belt saturation $S_0 = 40$ % and with inertia

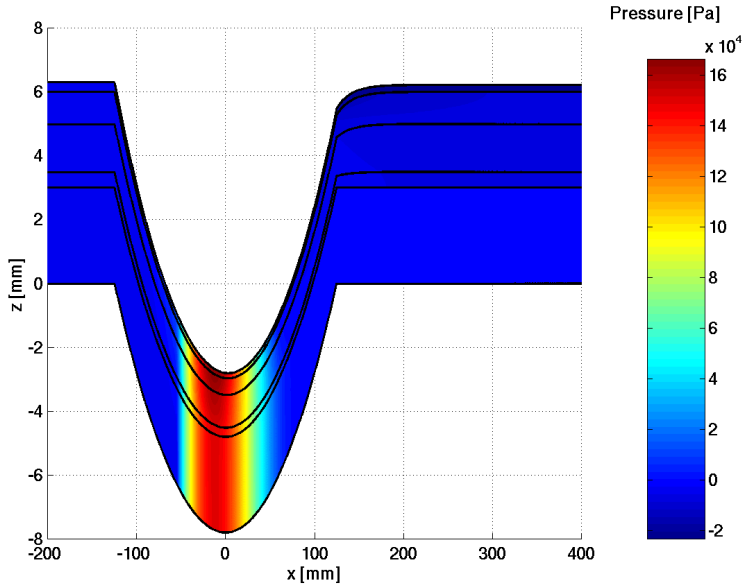

Figure 39: Pressure: $\mathbf{v}_s = 1250$ m/min, initial belt saturation $S_0 = 40$ % and with inertia

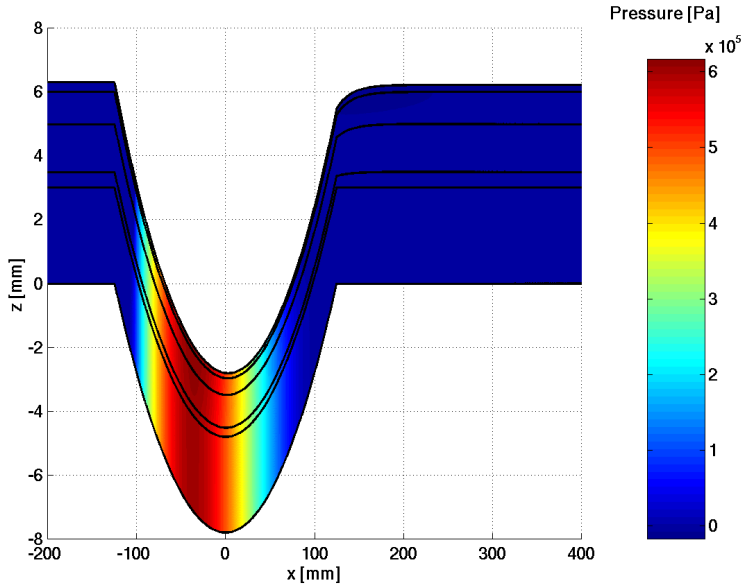

Figure 40: Pressure: $\mathbf{v}_s = 1250$ m/min, initial belt saturation $S_0 = 60$ % and with inertia

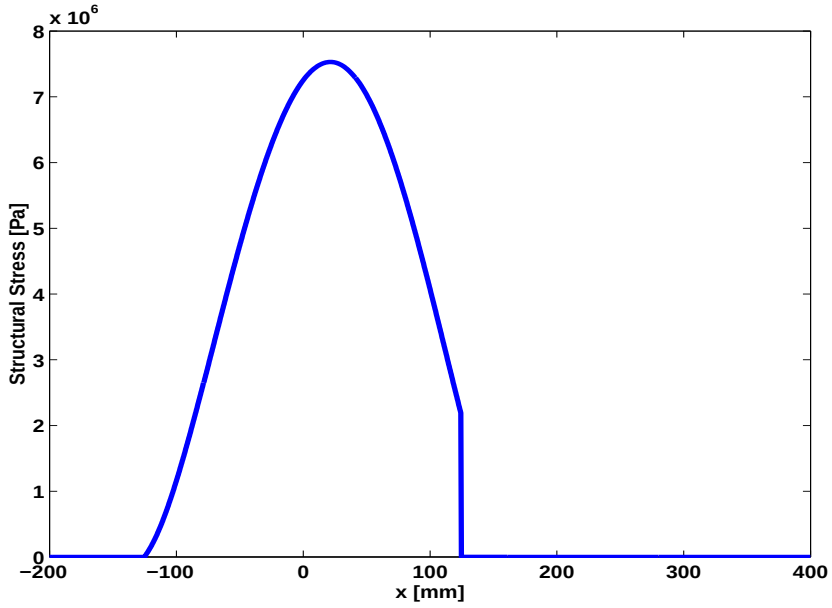

Figure 41: Structural stress: $\mathbf{v}_s = 750$ m/min

6 Conclusions

We developed a two dimensional model of the pressing section of a paper machine. The model accounts for the viscoelastic deformation of paper and felt layers and contains a macroscopic flow description including nonlinear filtration laws. Major effort went into the development of a suitable numerical solution algorithm which is based on a finite element discretization. Numerical results exhibit reasonable elastic and fluid dynamical behavior of the model in various setups. The choice of the flow parameters of the model was strongly influenced by computations using a three-dimensional virtual felt. We determined permeabilities and the nonlinear flow regime. The application of nonlinear filtration laws shows a major impact on the hydrodynamic pressure, which increases significantly. Hence, the hydrodynamic stress contribution being small in the Darcy regime should not be neglected in the elastic model, when considering high machine speeds.

References

[1] M. Allen, G. Behie, J. Trangenstein, *Multiphase flow in porous media*, Springer, Berlin, 1988.

[2] D.A. Anderson, J.C. Tannehill, R.H. Pletcher, *Computational fluid mechanics and heat transfer*, Hemisphere publ., New York, 1984.

[3] J. Bear, *Dynamics of fluids in porous media*, American Elsevier, 1972.

[4] J. Bear, A. Verruijt, *Modeling groundwater flow and pollution*, D. Reidel Publishing Company, 1987.

[5] J. Bear, Y. Bachmat, *Introduction to modeling of transport phenomena in porous media*, Kluwer, Dordrecht, 1990.

[6] J.W. Demmel, S.C. Eisenstat, J.R. Gilbert, X.S. Li, Joseph W.H. Liu, *A supernodal approach to sparse partial pivoting*, SIAM J. Matrix Analysis and Applications, Vol. 20, No. 3, pp. 720-755, 1999.

[7] A.D. Fitt, P.D. Howell, J.R. King, C.P. Please and D.W. Schwendeman, *Multiphase flow in a roll press nip*, European Journal of Applied Mathematics, 13. pp. 225-259, 2002.

[8] K. Hiltunen, *Mathematical and numerical modelling of consolidation processes in paper machines*, Thesis, University of Jyvaskyla, 1995.

[9] K. Jewett, W. Ceckler, L. Busker, and A. Co, *Computer model of a transversal flow nip*, AIChE Symposium Series 76 (200), pp. 59-70, New York, 1980.

[10] J. Tinsley Oden, G.F.Carey, *Finite Elements Volume I*, Prentice-Hall, Inc., 1984.

[11] S. Rief, *Nonlinear flow in porous media*, Dissertation, Universität Kaiserslautern, Germany, 2005.

[12] E. Sanchez-Palencia, *Non-homogeneous media and vibration theory*, Lecture Notes in Physics 127, Springer, 1980.

[13] X. Thibault, *Contribution à l'étude de structures tissées déformables: Application à l'évaluation du tenseur perméabilité des feutres de presses de papeterie*, Thesis, Institut National Polytechnique de Grenoble, 2001.

[14] K. Velten, W. Best, *Rolling of unsaturated porous materials: Evolution of a fully saturated zone*, Physical Review E, Vol. 62, No. 3, 2000.

Published reports of the Fraunhofer ITWM

The PDF-files of the following reports are available under:
www.itwm.fraunhofer.de/de/zentral__berichte/berichte

1. D. Hietel, K. Steiner, J. Struckmeier
A Finite - Volume Particle Method for Compressible Flows
(19 pages, 1998)

2. M. Feldmann, S. Seibold
Damage Diagnosis of Rotors: Application of Hilbert Transform and Multi-Hypothesis Testing
Keywords: Hilbert transform, damage diagnosis, Kalman filtering, non-linear dynamics
(23 pages, 1998)

3. Y. Ben-Haim, S. Seibold
Robust Reliability of Diagnostic Multi-Hypothesis Algorithms: Application to Rotating Machinery
Keywords: Robust reliability, convex models, Kalman filtering, multi-hypothesis diagnosis, rotating machinery, crack diagnosis
(24 pages, 1998)

4. F.-Th. Lentes, N. Siedow
Three-dimensional Radiative Heat Transfer in Glass Cooling Processes
(23 pages, 1998)

5. A. Klar, R. Wegener
A hierarchy of models for multilane vehicular traffic
Part I: Modeling
(23 pages, 1998)

Part II: Numerical and stochastic investigations
(17 pages, 1998)

6. A. Klar, N. Siedow
Boundary Layers and Domain Decomposition for Radiative Heat Transfer and Diffusion Equations: Applications to Glass Manufacturing Processes
(24 pages, 1998)

7. I. Choquet
Heterogeneous catalysis modelling and numerical simulation in rarified gas flows Part I: Coverage locally at equilibrium
(24 pages, 1998)

8. J. Ohser, B. Steinbach, C. Lang
Efficient Texture Analysis of Binary Images
(17 pages, 1998)

9. J. Orlik
Homogenization for viscoelasticity of the integral type with aging and shrinkage
(20 pages, 1998)

10. J. Mohring
Helmholtz Resonators with Large Aperture
(21 pages, 1998)

11. H. W. Hamacher, A. Schöbel
On Center Cycles in Grid Graphs
(15 pages, 1998)

12. H. W. Hamacher, K.-H. Küfer
Inverse radiation therapy planning - a multiple objective optimisation approach
(14 pages, 1999)

13. C. Lang, J. Ohser, R. Hilfer
On the Analysis of Spatial Binary Images
(20 pages, 1999)

14. M. Junk
On the Construction of Discrete Equilibrium Distributions for Kinetic Schemes
(24 pages, 1999)

15. M. Junk, S. V. Raghurame Rao
A new discrete velocity method for Navier-Stokes equations
(20 pages, 1999)

16. H. Neunzert
Mathematics as a Key to Key Technologies
(39 pages (4 PDF-Files), 1999)

17. J. Ohser, K. Sandau
Considerations about the Estimation of the Size Distribution in Wicksell's Corpuscle Problem
(18 pages, 1999)

18. E. Carrizosa, H. W. Hamacher, R. Klein, S. Nickel
Solving nonconvex planar location problems by finite dominating sets
Keywords: Continuous Location, Polyhedral Gauges, Finite Dominating Sets, Approximation, Sandwich Algorithm, Greedy Algorithm
(19 pages, 2000)

19. A. Becker
A Review on Image Distortion Measures
Keywords: Distortion measure, human visual system
(26 pages, 2000)

20. H. W. Hamacher, M. Labbé, S. Nickel, T. Sonneborn
Polyhedral Properties of the Uncapacitated Multiple Allocation Hub Location Problem
Keywords: integer programming, hub location, facility location, valid inequalities, facets, branch and cut
(21 pages, 2000)

21. H. W. Hamacher, A. Schöbel
Design of Zone Tariff Systems in Public Transportation
(30 pages, 2001)

22. D. Hietel, M. Junk, R. Keck, D. Teleaga
The Finite-Volume-Particle Method for Conservation Laws
(16 pages, 2001)

23. T. Bender, H. Hennes, J. Kalcsics, M. T. Melo, S. Nickel
Location Software and Interface with GIS and Supply Chain Management
Keywords: facility location, software development, geographical information systems, supply chain management
(48 pages, 2001)

24. H. W. Hamacher, S. A. Tjandra
Mathematical Modelling of Evacuation Problems: A State of Art
(44 pages, 2001)

25. J. Kuhnert, S. Tiwari
Grid free method for solving the Poisson equation
Keywords: Poisson equation, Least squares method, Grid free method
(19 pages, 2001)

26. T. Götz, H. Rave, D. Reinel-Bitzer, K. Steiner, H. Tiemeier
Simulation of the fiber spinning process
Keywords: Melt spinning, fiber model, Lattice Boltzmann, CFD
(19 pages, 2001)

27. A. Zemitis
On interaction of a liquid film with an obstacle
Keywords: impinging jets, liquid film, models, numerical solution, shape
(22 pages, 2001)

28. I. Ginzburg, K. Steiner
Free surface lattice-Boltzmann method to model the filling of expanding cavities by Bingham Fluids
Keywords: Generalized LBE, free-surface phenomena, interface boundary conditions, filling processes, Bingham viscoplastic model, regularized models
(22 pages, 2001)

29. H. Neunzert
»Denn nichts ist für den Menschen als Menschen etwas wert, was er nicht mit Leidenschaft tun kann«
Vortrag anlässlich der Verleihung des Akademiepreises des Landes Rheinland-Pfalz am 21.11.2001
Keywords: Lehre, Forschung, angewandte Mathematik, Mehrskalenanalyse, Strömungsmechanik
(18 pages, 2001)

30. J. Kuhnert, S. Tiwari
Finite pointset method based on the projection method for simulations of the incompressible Navier-Stokes equations
Keywords: Incompressible Navier-Stokes equations, Meshfree method, Projection method, Particle scheme, Least squares approximation
AMS subject classification: 76D05, 76M28
(25 pages, 2001)

31. R. Korn, M. Krekel
Optimal Portfolios with Fixed Consumption or Income Streams
Keywords: Portfolio optimisation, stochastic control, HJB equation, discretisation of control problems.
(23 pages, 2002)

32. M. Krekel
Optimal portfolios with a loan dependent credit spread
Keywords: Portfolio optimisation, stochastic control, HJB equation, credit spread, log utility, power utility, non-linear wealth dynamics
(25 pages, 2002)

33. J. Ohser, W. Nagel, K. Schladitz
The Euler number of discretized sets – on the choice of adjacency in homogeneous lattices
Keywords: image analysis, Euler number, neighborhod relationships, cuboidal lattice
(32 pages, 2002)

34. I. Ginzburg, K. Steiner

Lattice Boltzmann Model for Free-Surface flow and Its Application to Filling Process in Casting

Keywords: Lattice Boltzmann models; free-surface phenomena; interface boundary conditions; filling processes; injection molding; volume of fluid method; interface boundary conditions; advection-schemes; upwind-schemes
(54 pages, 2002)

35. M. Günther, A. Klar, T. Materne, R. Wegener

Multivalued fundamental diagrams and stop and go waves for continuum traffic equations

Keywords: traffic flow, macroscopic equations, kinetic derivation, multivalued fundamental diagram, stop and go waves, phase transitions
(25 pages, 2002)

36. S. Feldmann, P. Lang, D. Prätzel-Wolters

Parameter influence on the zeros of network determinants

Keywords: Networks, Equicofactor matrix polynomials, Realization theory, Matrix perturbation theory
(30 pages, 2002)

37. K. Koch, J. Ohser, K. Schladitz

Spectral theory for random closed sets and estimating the covariance via frequency space

Keywords: Random set, Bartlett spectrum, fast Fourier transform, power spectrum
(28 pages, 2002)

38. D. d'Humières, I. Ginzburg

Multi-reflection boundary conditions for lattice Boltzmann models

Keywords: lattice Boltzmann equation, boudary condistions, bounce-back rule, Navier-Stokes equation
(72 pages, 2002)

39. R. Korn

Elementare Finanzmathematik

Keywords: Finanzmathematik, Aktien, Optionen, Portfolio-Optimierung, Börse, Lehrerweiterbildung, Mathematikunterricht
(98 pages, 2002)

40. J. Kallrath, M. C. Müller, S. Nickel

Batch Presorting Problems: Models and Complexity Results

Keywords: Complexity theory, Integer programming, Assigment, Logistics
(19 pages, 2002)

41. J. Linn

On the frame-invariant description of the phase space of the Folgar-Tucker equation

Key words: fiber orientation, Folgar-Tucker equation, injection molding
(5 pages, 2003)

42. T. Hanne, S. Nickel

A Multi-Objective Evolutionary Algorithm for Scheduling and Inspection Planning in Software Development Projects

Key words: multiple objective programming, project management and scheduling, software development, evolutionary algorithms, efficient set
(29 pages, 2003)

43. T. Bortfeld , K.-H. Küfer, M. Monz, A. Scherrer, C. Thieke, H. Trinkaus

Intensity-Modulated Radiotherapy - A Large Scale Multi-Criteria Programming Problem

Keywords: multiple criteria optimization, representative systems of Pareto solutions, adaptive triangulation, clustering and disaggregation techniques, visualization of Pareto solutions, medical physics, external beam radiotherapy planning, intensity modulated radiotherapy
(31 pages, 2003)

44. T. Halfmann, T. Wichmann

Overview of Symbolic Methods in Industrial Analog Circuit Design

Keywords: CAD, automated analog circuit design, symbolic analysis, computer algebra, behavioral modeling, system simulation, circuit sizing, macro modeling, differential-algebraic equations, index
(17 pages, 2003)

45. S. E. Mikhailov, J. Orlik

Asymptotic Homogenisation in Strength and Fatigue Durability Analysis of Composites

Keywords: multiscale structures, asymptotic homogenization, strength, fatigue, singularity, non-local conditions
(14 pages, 2003)

46. P. Domínguez-Marín, P. Hansen, N. Mladenovi´c , S. Nickel

Heuristic Procedures for Solving the Discrete Ordered Median Problem

Keywords: genetic algorithms, variable neighborhood search, discrete facility location
(31 pages, 2003)

47. N. Boland, P. Domínguez-Marín, S. Nickel, J. Puerto

Exact Procedures for Solving the Discrete Ordered Median Problem

Keywords: discrete location, Integer programming
(41 pages, 2003)

48. S. Feldmann, P. Lang

Padé-like reduction of stable discrete linear systems preserving their stability

Keywords: Discrete linear systems, model reduction, stability, Hankel matrix, Stein equation
(16 pages, 2003)

49. J. Kallrath, S. Nickel

A Polynomial Case of the Batch Presorting Problem

Keywords: batch presorting problem, online optimization, competetive analysis, polynomial algorithms, logistics
(17 pages, 2003)

50. T. Hanne, H. L. Trinkaus

knowCube for MCDM – Visual and Interactive Support for Multicriteria Decision Making

Key words: Multicriteria decision making, knowledge management, decision support systems, visual interfaces, interactive navigation, real-life applications.
(26 pages, 2003)

51. O. Iliev, V. Laptev

On Numerical Simulation of Flow Through Oil Filters

Keywords: oil filters, coupled flow in plain and porous media, Navier-Stokes, Brinkman, numerical simulation
(8 pages, 2003)

52. W. Dörfler, O. Iliev, D. Stoyanov, D. Vassileva

On a Multigrid Adaptive Refinement Solver for Saturated Non-Newtonian Flow in Porous Media

Keywords: Nonlinear multigrid, adaptive refinement, non-Newtonian flow in porous media
(17 pages, 2003)

53. S. Kruse

On the Pricing of Forward Starting Options under Stochastic Volatility

Keywords: Option pricing, forward starting options, Heston model, stochastic volatility, cliquet options
(11 pages, 2003)

54. O. Iliev, D. Stoyanov

Multigrid – adaptive local refinement solver for incompressible flows

Keywords: Navier-Stokes equations, incompressible flow, projection-type splitting, SIMPLE, multigrid methods, adaptive local refinement, lid-driven flow in a cavity
(37 pages, 2003)

55. V. Starikovicius

The multiphase flow and heat transfer in porous media

Keywords: Two-phase flow in porous media, various formulations, global pressure, multiphase mixture model, numerical simulation
(30 pages, 2003)

56. P. Lang, A. Sarishvili, A. Wirsen

Blocked neural networks for knowledge extraction in the software development process

Keywords: Blocked Neural Networks, Nonlinear Regression, Knowledge Extraction, Code Inspection
(21 pages, 2003)

57. H. Knaf, P. Lang, S. Zeiser

Diagnosis aiding in Regulation Thermography using Fuzzy Logic

Keywords: fuzzy logic,knowledge representation, expert system
(22 pages, 2003)

58. M. T. Melo, S. Nickel, F. Saldanha da Gama

Largescale models for dynamic multicommodity capacitated facility location

Keywords: supply chain management, strategic planning, dynamic location, modeling
(40 pages, 2003)

59. J. Orlik

Homogenization for contact problems with periodically rough surfaces

Keywords: asymptotic homogenization, contact problems
(28 pages, 2004)

60. A. Scherrer, K.-H. Küfer, M. Monz, F. Alonso, T. Bortfeld

IMRT planning on adaptive volume structures – a significant advance of computational complexity

Keywords: Intensity-modulated radiation therapy (IMRT), inverse treatment planning, adaptive volume structures, hierarchical clustering, local refinement, adaptive clustering, convex programming, mesh generation, multi-grid methods
(24 pages, 2004)

61. D. Kehrwald

Parallel lattice Boltzmann simulation of complex flows

Keywords: Lattice Boltzmann methods, parallel computing, microstructure simulation, virtual material design, pseudo-plastic fluids, liquid composite moulding
(12 pages, 2004)

62. O. Iliev, J. Linn, M. Moog, D. Niedziela, V. Starikovicius

On the Performance of Certain Iterative Solvers for Coupled Systems Arising in Discretization of Non-Newtonian Flow Equations

Keywords: Performance of iterative solvers, Preconditioners, Non-Newtonian flow
(17 pages, 2004)

63. R. Ciegis, O. Iliev, S. Rief, K. Steiner

On Modelling and Simulation of Different Regimes for Liquid Polymer Moulding

Keywords: Liquid Polymer Moulding, Modelling, Simulation, Infiltration, Front Propagation, non-Newtonian flow in porous media
(43 pages, 2004)

64. T. Hanne, H. Neu

Simulating Human Resources in Software Development Processes

Keywords: Human resource modeling, software process, productivity, human factors, learning curve
(14 pages, 2004)

65. O. Iliev, A. Mikelic, P. Popov

Fluid structure interaction problems in deformable porous media: Toward permeability of deformable porous media

Keywords: fluid-structure interaction, deformable porous media, upscaling, linear elasticity, stokes, finite elements
(28 pages, 2004)

66. F. Gaspar, O. Iliev, F. Lisbona, A. Naumovich, P. Vabishchevich

On numerical solution of 1-D poroelasticity equations in a multilayered domain

Keywords: poroelasticity, multilayered material, finite volume discretization, MAC type grid
(41 pages, 2004)

67. J. Ohser, K. Schladitz, K. Koch, M. Nöthe

Diffraction by image processing and its application in materials science

Keywords: porous microstructure, image analysis, random set, fast Fourier transform, power spectrum, Bartlett spectrum
(13 pages, 2004)

68. H. Neunzert

Mathematics as a Technology: Challenges for the next 10 Years

Keywords: applied mathematics, technology, modelling, simulation, visualization, optimization, glass processing, spinning processes, fiber-fluid interaction, trubulence effects, topological optimization, multicriteria optimization, Uncertainty and Risk, financial mathematics, Malliavin calculus, Monte-Carlo methods, virtual material design, filtration, bio-informatics, system biology
(29 pages, 2004)

69. R. Ewing, O. Iliev, R. Lazarov, A. Naumovich

On convergence of certain finite difference discretizations for 1D poroelasticity interface problems

Keywords: poroelasticity, multilayered material, finite volume discretizations, MAC type grid, error estimates
(26 pages,2004)

70. W. Dörfler, O. Iliev, D. Stoyanov, D. Vassileva

On Efficient Simulation of Non-Newtonian Flow in Saturated Porous Media with a Multigrid Adaptive Refinement Solver

Keywords: Nonlinear multigrid, adaptive renement, non-Newtonian in porous media
(25 pages, 2004)

71. J. Kalcsics, S. Nickel, M. Schröder

Towards a Unified Territory Design Approach – Applications, Algorithms and GIS Integration

Keywords: territory desgin, political districting, sales territory alignment, optimization algorithms, Geographical Information Systems
(40 pages, 2005)

72. K. Schladitz, S. Peters, D. Reinel-Bitzer, A. Wiegmann, J. Ohser

Design of acoustic trim based on geometric modeling and flow simulation for non-woven

Keywords: random system of fibers, Poisson line process, flow resistivity, acoustic absorption, Lattice-Boltzmann method, non-woven
(21 pages, 2005)

73. V. Rutka, A. Wiegmann

Explicit Jump Immersed Interface Method for virtual material design of the effective elastic moduli of composite materials

Keywords: virtual material design, explicit jump immersed interface method, effective elastic moduli, composite materials
(22 pages, 2005)

74. T. Hanne

Eine Übersicht zum Scheduling von Baustellen

Keywords: Projektplanung, Scheduling, Bauplanung, Bauindustrie
(32 pages, 2005)

75. J. Linn

The Folgar-Tucker Model as a Differetial Algebraic System for Fiber Orientation Calculation

Keywords: fiber orientation, Folgar–Tucker model, invariants, algebraic constraints, phase space, trace stability
(15 pages, 2005)

76. M. Speckert, K. Dreßler, H. Mauch, A. Lion, G. J. Wierda

Simulation eines neuartigen Prüfsystems für Achserprobungen durch MKS-Modellierung einschließlich Regelung

Keywords: virtual test rig, suspension testing, multibody simulation, modeling hexapod test rig, optimization of test rig configuration
(20 pages, 2005)

77. K.-H. Küfer, M. Monz, A. Scherrer, P. Süss, F. Alonso, A. S. A. Sultan, Th. Bortfeld, D. Craft, Chr. Thieke

Multicriteria optimization in intensity modulated radiotherapy planning

Keywords: multicriteria optimization, extreme solutions, real-time decision making, adaptive approximation schemes, clustering methods, IMRT planning, reverse engineering
(51 pages, 2005)

78. S. Amstutz, H. Andrä

A new algorithm for topology optimization using a level-set method

Keywords: shape optimization, topology optimization, topological sensitivity, level-set
(22 pages, 2005)

79. N. Ettrich

Generation of surface elevation models for urban drainage simulation

Keywords: Flooding, simulation, urban elevation models, laser scanning
(22 pages, 2005)

80. H. Andrä, J. Linn, I. Matei, I. Shklyar, K. Steiner, E. Teichmann

OPTCAST – Entwicklung adäquater Strukturoptimierungsverfahren für Gießereien Technischer Bericht (KURZFASSUNG)

Keywords: Topologieoptimierung, Level-Set-Methode, Gießprozesssimulation, Gießtechnische Restriktionen, CAE-Kette zur Strukturoptimierung
(77 pages, 2005)

81. N. Marheineke, R. Wegener

Fiber Dynamics in Turbulent Flows Part I: General Modeling Framework

Keywords: fiber-fluid interaction; Cosserat rod; turbulence modeling; Kolmogorov's energy spectrum; double-velocity correlations; differentiable Gaussian fields
(20 pages, 2005)

Part II: Specific Taylor Drag

Keywords: flexible fibers; k-ε turbulence model; fiber-turbulence interaction scales; air drag; random Gaussian aerodynamic force; white noise; stochastic differential equations; ARMA process
(18 pages, 2005)

82. C. H. Lampert, O. Wirjadi

An Optimal Non-Orthogonal Separation of the Anisotropic Gaussian Convolution Filter

Keywords: Anisotropic Gaussian filter, linear filtering, orientation space, nD image processing, separable filters
(25 pages, 2005)

83. H. Andrä, D. Stoyanov

Error indicators in the parallel finite element solver for linear elasticity DDFEM

Keywords: linear elasticity, finite element method, hierarchical shape functions, domain decom-position, parallel implementation, a posteriori error estimates
(21 pages, 2006)

84. M. Schröder, I. Solchenbach

Optimization of Transfer Quality in Regional Public Transit

Keywords: public transit, transfer quality, quadratic assignment problem
(16 pages, 2006)

85. A. Naumovich, F. J. Gaspar

On a multigrid solver for the three-dimensional Biot poroelasticity system in multilayered domains

Keywords: poroelasticity, interface problem, multigrid, operator-dependent prolongation
(11 pages, 2006)

86. S. Panda, R. Wegener, N. Marheineke

Slender Body Theory for the Dynamics of Curved Viscous Fibers

Keywords: curved viscous fibers; fluid dynamics; Navier-Stokes equations; free boundary value problem; asymptotic expansions; slender body theory
(14 pages, 2006)

87. E. Ivanov, H. Andrä, A. Kudryavtsev

Domain Decomposition Approach for Automatic Parallel Generation of Tetrahedral Grids

Key words: Grid Generation, Unstructured Grid, Delaunay Triangulation, Parallel Programming, Domain Decomposition, Load Balancing
(18 pages, 2006)

88. S. Tiwari, S. Antonov, D. Hietel, J. Kuhnert, R. Wegener

A Meshfree Method for Simulations of Interactions between Fluids and Flexible Structures

Key words: Meshfree Method, FPM, Fluid Structure Interaction, Sheet of Paper, Dynamical Coupling
(16 pages, 2006)

89. R. Ciegis , O. Iliev, V. Starikovicius, K. Steiner

Numerical Algorithms for Solving Problems of Multiphase Flows in Porous Media

Keywords: nonlinear algorithms, finite-volume method, software tools, porous media, flows
(16 pages, 2006)

90. D. Niedziela, O. Iliev, A. Latz

On 3D Numerical Simulations of Viscoelastic Fluids

Keywords: non-Newtonian fluids, anisotropic viscosity, integral constitutive equation
(18 pages, 2006)

91. A. Winterfeld

Application of general semi-infinite Programming to Lapidary Cutting Problems

Keywords: large scale optimization, nonlinear programming, general semi-infinite optimization, design centering, clustering
(26 pages, 2006)

92. J. Orlik, A. Ostrovska

Space-Time Finite Element Approximation and Numerical Solution of Hereditary Linear Viscoelasticity Problems

Keywords: hereditary viscoelasticity; kern approximation by interpolation; space-time finite element approximation, stability and a priori estimate
(24 pages, 2006)

93. V. Rutka, A. Wiegmann, H. Andrä

EJIIM for Calculation of effective Elastic Moduli in 3D Linear Elasticity

Keywords: Elliptic PDE, linear elasticity, irregular domain, finite differences, fast solvers, effective elastic moduli
(24 pages, 2006)

94. A. Wiegmann, A. Zemitis

EJ-HEAT: A Fast Explicit Jump Harmonic Averaging Solver for the Effective Heat Conductivity of Composite Materials

Keywords: Stationary heat equation, effective thermal conductivity, explicit jump, discontinuous coefficients, virtual material design, microstructure simulation, EJ-HEAT
(21 pages, 2006)

95. A. Naumovich

On a finite volume discretization of the three-dimensional Biot poroelasticity system in multilayered domains

Keywords: Biot poroelasticity system, interface problems, finite volume discretization, finite difference method.
(21 pages, 2006)

96. M. Krekel, J. Wenzel

A unified approach to Credit Default Swaption and Constant Maturity Credit Default Swap valuation

Keywords: LIBOR market model, credit risk, Credit Default Swaption, Constant Maturity Credit Default Swap-method.
(43 pages, 2006)

97. A. Dreyer

Interval Methods for Analog Circiuts

Keywords: interval arithmetic, analog circuits, tolerance analysis, parametric linear systems, frequency response, symbolic analysis, CAD, computer algebra
(36 pages, 2006)

98. N. Weigel, S. Weihe, G. Bitsch, K. Dreßler

Usage of Simulation for Design and Optimization of Testing

Keywords: Vehicle test rigs, MBS, control, hydraulics, testing philosophy
(14 pages, 2006)

99. H. Lang, G. Bitsch, K. Dreßler, M. Speckert

Comparison of the solutions of the elastic and elastoplastic boundary value problems

Keywords: Elastic BVP, elastoplastic BVP, variational inequalities, rate-independency, hysteresis, linear kinematic hardening, stop- and play-operator
(21 pages, 2006)

100. M. Speckert, K. Dreßler, H. Mauch

MBS Simulation of a hexapod based suspension test rig

Keywords: Test rig, MBS simulation, suspension, hydraulics, controlling, design optimization
(12 pages, 2006)

101. S. Azizi Sultan, K.-H. Küfer

A dynamic algorithm for beam orientations in multicriteria IMRT planning

Keywords: radiotherapy planning, beam orientation optimization, dynamic approach, evolutionary algorithm, global optimization
(14 pages, 2006)

102. T. Götz, A. Klar, N. Marheineke, R. Wegener

A Stochastic Model for the Fiber Lay-down Process in the Nonwoven Production

Keywords: fiber dynamics, stochastic Hamiltonian system, stochastic averaging
(17 pages, 2006)

103. Ph. Süss, K.-H. Küfer

Balancing control and simplicity: a variable aggregation method in intensity modulated radiation therapy planning

Keywords: IMRT planning, variable aggregation, clustering methods
(22 pages, 2006)

104. A. Beaudry, G. Laporte, T. Melo, S. Nickel

Dynamic transportation of patients in hospitals

Keywords: in-house hospital transportation, dial-a-ride, dynamic mode, tabu search
(37 pages, 2006)

105. Th. Hanne

Applying multiobjective evolutionary algorithms in industrial projects

Keywords: multiobjective evolutionary algorithms, discrete optimization, continuous optimization, electronic circuit design, semi-infinite programming, scheduling
(18 pages, 2006)

106. J. Franke, S. Halim

Wild bootstrap tests for comparing signals and images

Keywords: wild bootstrap test, texture classification, textile quality control, defect detection, kernel estimate, nonparametric regression
(13 pages, 2007

107. Z. Drezner, S. Nickel

Solving the ordered one-median problem in the plane

Keywords: planar location, global optimization, ordered median, big triangle small triangle method, bounds, numerical experiments
(21 pages, 2007)

108. Th. Götz, A. Klar, A. Unterreiter, R. Wegener

Numerical evidance for the non-existing of solutions of the equations desribing rotational fiber spinning

Keywords: rotational fiber spinning, viscous fibers, boundary value problem, existence of solutions
(11 pages, 2007)

109. Ph. Süss, K.-H. Küfer

Smooth intensity maps and the Bortfeld-Boyer sequencer

Keywords: probabilistic analysis, intensity modulated radiotherapy treatment (IMRT), IMRT plan application, step-and-shoot sequencing
(8 pages, 2007)

110. E. Ivanov, O. Gluchshenko, H. Andrä, A. Kudryavtsev

Parallel software tool for decomposing and meshing of 3d structures

Keywords: a-priori domain decomposition, unstructured grid, Delaunay mesh generation
(14 pages, 2007)

111. O. Iliev, R. Lazarov, J. Willems

Numerical study of two-grid preconditioners for 1d elliptic problems with highly oscillating discontinuous coefficients

Keywords: two-grid algorithm, oscillating coefficients, preconditioner
(20 pages, 2007)

112. L. Bonilla, T. Götz, A. Klar, N. Marheineke, R. Wegener

Hydrodynamic limit of the Fokker-Planck-equation describing fiber lay-down processes

Keywords: stochastic dierential equations, Fokker-Planck equation, asymptotic expansion, Ornstein-Uhlenbeck process
(17 pages, 2007)

113. S. Rief

Modeling and simulation of the pressing section of a paper machine

Keywords: paper machine, computational fluid dynamics, porous media
(41 pages, 2007)

Status quo: May 2007